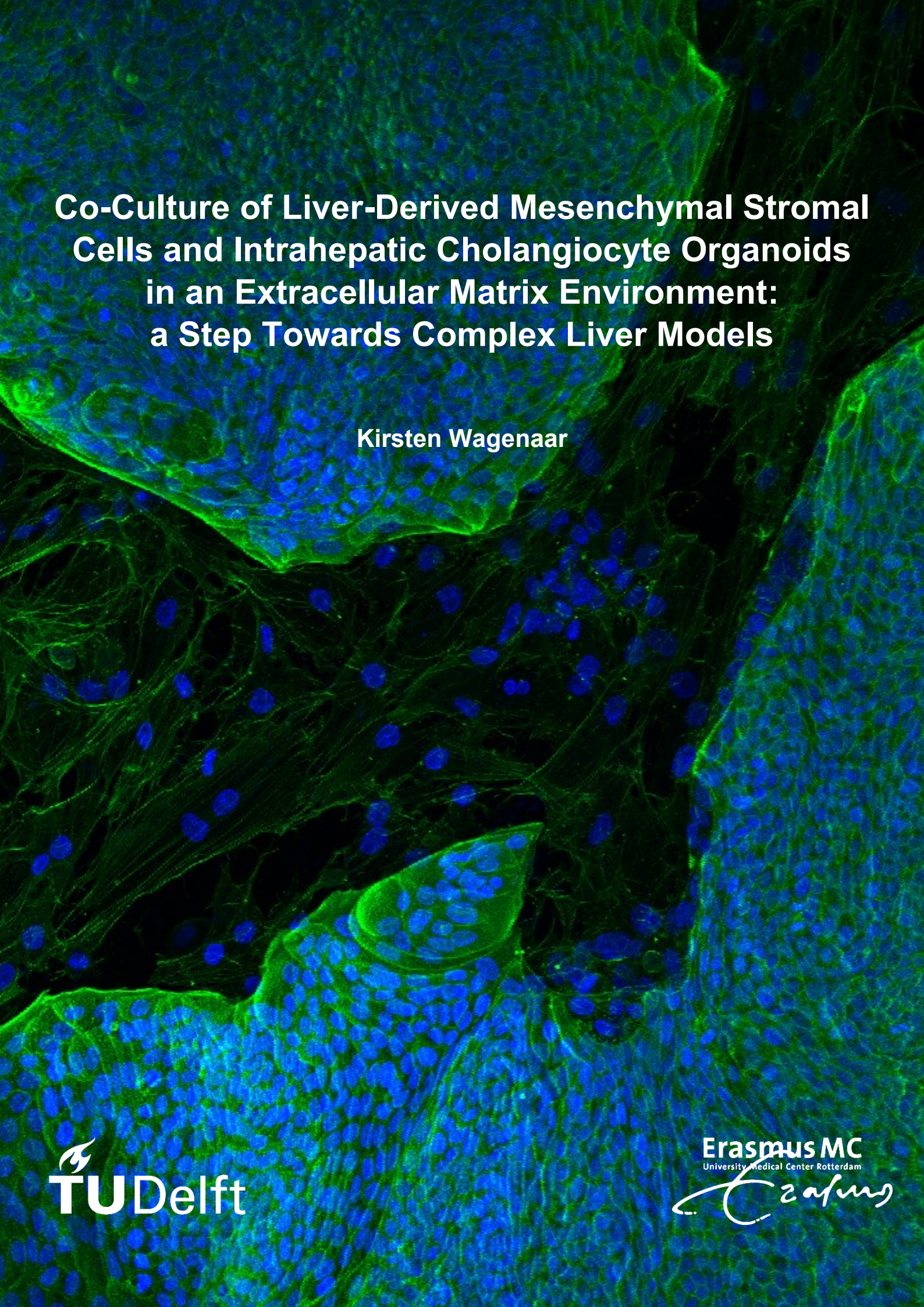

Co-Culture of Liver-Derived Mesenchymal Stromal Cells and Intrahepatic Cholangiocyte Organoids in an Extracellular Matrix Environment: a Step Towards Complex Liver Models

Kirsten Wagenaar

TU Delft

Erasmus MC
University Medical Center Rotterdam

Co-Culture of Liver-Derived Mesenchymal Stromal Cells and Intrahepatic Cholangiocyte Organoids in an Extracellular Matrix Environment: a Step Towards Complex Liver Models

By

Kirsten Wagenaar

to obtain the degree of Master of Science at the Delft University of Technology

Student number:	4381661	
Daily supervisor:	J. Willemse, MSc	Erasmus MC
Thesis supervisors:	Dr. M.M.A. Verstegen	Erasmus MC
	Prof. dr. L.J.W. van der Laan	Erasmus MC
	Dr. Ir. E. L. Fratila-Apachitei	TU Delft
	Prof. dr. A. A. Zadpoor	TU Delft
Department:	Laboratory of Experimental Transplantation and Intestinal Surgery (LETIS) at the department of Surgery of the Erasmus MC	

An electronic version of this thesis is available at http://repository.tudelft.nl/.

TU Delft

Abstract

To this day, liver transplantation is the only effective treatment for end-stage liver failure. Unfortunately, the scarcity of liver donors leads to waitlist mortality, pushing the need for alternative treatment options. *In vitro* models are essential tools in research on alternatives for transplantation. One of the promising models is the hepatobiliary organoid model because these three-dimensional cultures model (elements of) the native tissue structure and function. However, a limitation of these models is that they currently resemble only one liver cell type. The aim of this research was therefore to combine different cell types, i.e., biliary organoids and mesenchymal stromal cells (MSCs), in one culture model.

The organoids were obtained from liver-biopsy-derived intrahepatic biliary epithelium and are therefore named intrahepatic cholangiocyte organoids (ICOs). The liver-specific MSCs (L-MSCs) were isolated from perfusion fluid of donor livers collected at liver transplantation procedures. Decellularized liver tissue was used to include extracellular matrix (ECM) in the co-culture models. To assess the most optimal culture conditions, three experimental setups were tested. In the first setup, ICOs were cultured in different concentrations of L-MSC derived conditioned medium (CM) in commercially available basement membrane extract (BME) (1A). This setup was also used to differentiated the ICOs towards hepatocytes (1B). In the second setup, various concentrations of ICOs and L-MSCs were cultured in an indirect (2A) and direct (2B) BME model. The third setup included liver-derived ECM to replace the BME. Cells were cultured similar to model 2B (3A) and ICOs were added after a pre-culture of L-MSCs (3B). The morphology of both cell types, the visible interaction between cell types, and the expression of hepatocyte, cholangiocyte, MSC and proliferation markers were analyzed.

The effect of L-MSCs and L-MSC-derived CM on ICO formation, morphology, and growth patterns, was small. Direct cell-cell contact was rare in the BME co-cultures, but instances of close contact between two cell types were observed in both the indirect (2A) and direct (2B) setups. In the ECM models (3A-B), ICO cells formed polarized monolayers that pushed the L-MSCs aside, indicating that the cell types did not mix well. ICOs expressed the cholangiocyte markers cytokeratin (CK) 7 and 19 in both mono- and co-cultures, whereas L-MSCs were most likely CK7 and CK19 negative. Variation in gene expression levels of hepatocyte, cholangiocyte, MSC, and proliferation markers was observed, but no statistically significant differences were found between conditions. Nevertheless, the down-regulatory effect of CM on the expression of hepatocyte markers in differentiated ICOs showed a consistent trend. Additionally, the presence of L-MSCs resulted in a higher mean expression of MSC markers CD90, CD105 and Vimentin, and proliferation marker KI-67.

Although no clear effects of L-MSCs on ICO growth were observed in this study, the created co-culture models form a promising base for future research. The models include adult human liver-derived components and are therefore a step towards the reconstruction of the hepatic microenvironment. In addition, if other (liver-derived) cell types were to be introduced to the co-culture models, L-MSCs have the potential to enhance the cell function of these new cells. Last, the models can be used as a base for future ICO co-culture studies, since the L-MSCs can be replaced by other cell types.

Graphical abstract

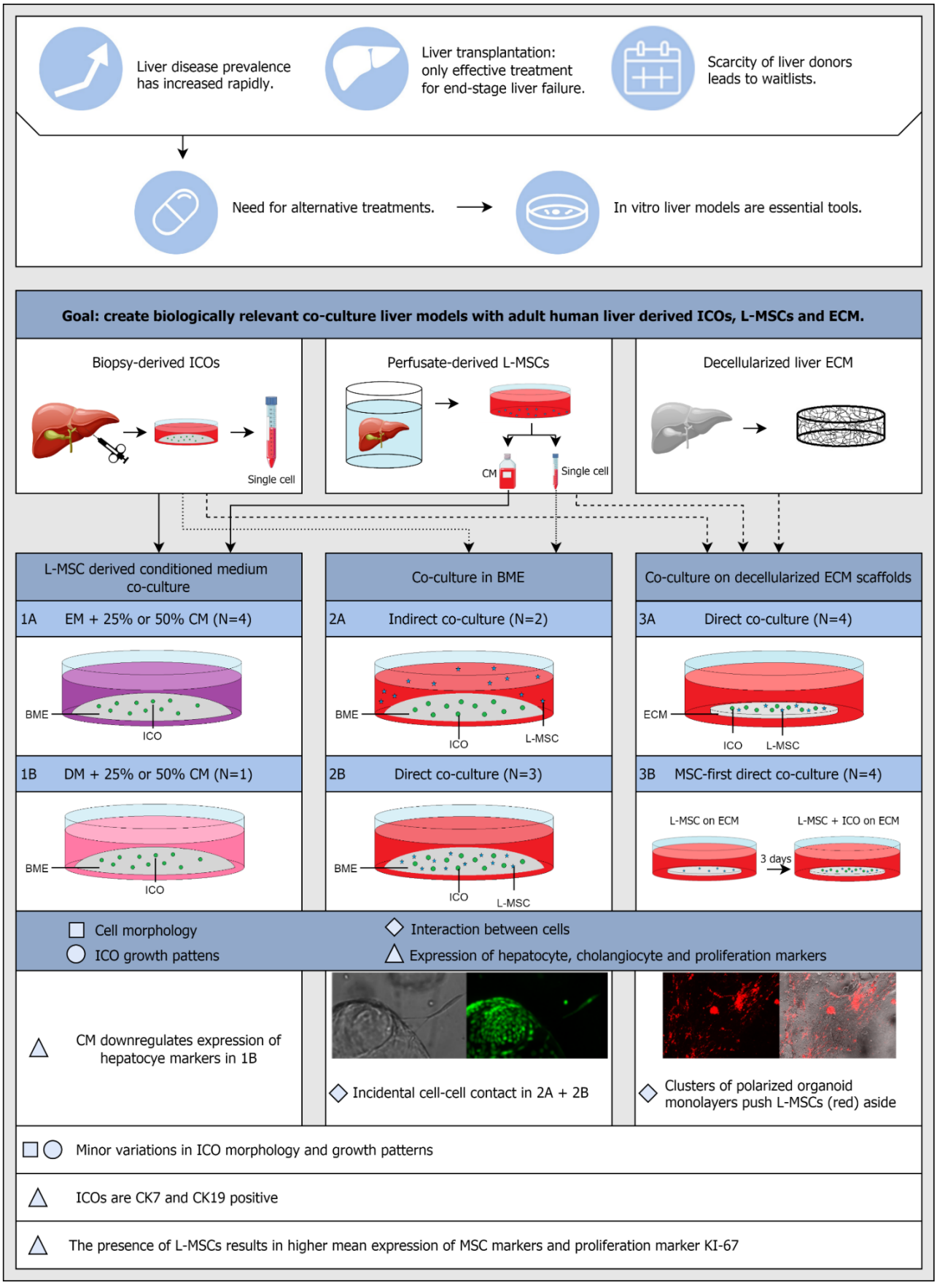

Contents

Abbreviations

BME	Basement Membrane Extract
cDNA	Complementary DNA
CK7	Cytokeratin 7
CK19	Cytokeratin 19
CM	Conditioned Medium
DM	Differentiation Medium (Appendix B)
EBD	Extrahepatic Bile Duct
ECM	Extracellular Matrix
EM	Expansion Medium (Appendix B)
H&E	Haematoxylin and Eosin
HUVEC	Human Umbilical Vein Endothelial Cell
HSC	Hepatic Stellate Cell
ICO	Intrahepatic Cholangiocyte Organoids
iPSC	Induced Pluripotent Stem Cell
L-MSC	Liver-Specific Mesenchymal Stromal Cell
LSEC	Liver Sinusoidal Endothelial Cell
MSC	Mesenchymal Stromal Cell
PFA	Paraformaldehyde
PI	Propidiumiodide
TE	Trypsin-EDTA (0.05%)
UW	University of Wisconsin Solution
qPCR	Quantitative Polymerase Chain Reaction

1 Introduction

The liver is a vital organ, performing processes related to digestion, metabolism, nutrient storage, detoxification, and immunity. A diseased liver can cause major health problems and can even result in death if the liver is damaged beyond repair (end-stage liver disease). In the past decades, liver disease prevalence has increased rapidly. In Europe alone, around 29 million people suffer from chronic liver diseases such as liver cancer and liver cirrhosis, often caused by harmful alcohol consumption, hepatitis B and C, and fatty liver [1]. Currently, the only treatment option for end-stage liver disease is liver transplantation. Unfortunately, the shortage of donor organs results in waitlist mortality.

To decrease the burden of (end-stage) liver disease and related deaths, alternative treatments are needed. A good understanding of healthy and diseased liver development and function is crucial. *In vitro* liver models play an important role by giving insight into behavior on cellular and tissue level. Moreover, models have the potential to be used for several clinical applications, like drug development and testing, personalized medicine, and tissue engineering. Because existing *in vitro* models have limitations and often resemble only a part of the liver tissue, research is constantly pushed to create physiologically more relevant models. To obtain these models, elements of the *in vivo* liver environment are recreated *in vitro*. This study focuses on three commonly used methods: culturing cells in a 3D environment, combining multiple cell types in one model (co-culture), and including non-cellular tissue components, i.e., extracellular matrix (ECM).

1.1 3D culture models: liver organoids

3D culture models are widely used to fill the gap between the “simple” 2D monolayer models and animal models. Compared to 2D models, 3D models resemble *in vivo* conditions more closely because cells have cell-cell and cell-ECM contact in all dimensions and are more exposed to medium concentration gradients [2]. A specific type of 3D model is the organoid model. This model is characterized by the capacity of epithelial cells to form self-organized 3D structures that emulate (elements of) the native tissue structure and function. Liver organoid models can be initiated with cells from varying origins: adult and fetal liver tissue [3,4] and pluripotent stromal cells [5–7]. In the presence of specific growth factors, cells can be stimulated to form long-term stable hepatic and biliary organoids.

1.1.1 Intrahepatic cholangiocyte organoids

A type of hepatobiliary organoid is the intrahepatic cholangiocyte organoid (ICO). ICOs are promising candidates for *in vitro* cholangiocyte modeling [4]. It is important to model the cholangiocytes since they form the inner lining of the bile ducts and perform key liver functions. In short, bile (produced by hepatocytes) is transported through the biliary tract towards the small intestine. The cholangiocytes modify the composition of the bile and protect the surrounding tissue [8]. Cholangiocytes are damaged in several chronic diseases, known as cholangiopathies. This damage impairs the bile composition and flow and can cause leakage and accumulation of bile. In the worst-case, the liver becomes irreparably damaged, and transplantation is needed [9].

ICOs can be initiated from human liver biopsies with high success rates [10]. The cells are EPCAM and LGR5 double-positive and form hollow spheroids when cultured in specialized expansion medium (EM) in hydrogel. ICOs maintain their genetic stability, allowing long-term culture. Because ICOs can also be derived from patient biopsies that maintain disease characteristics in culture, they are suitable to model numerous liver diseases. ICOs express cholangiocyte-specific markers as EPCAM and cytokeratin (CK) 7 and 19. In addition, the ICOs can be differentiated towards a hepatocyte-like phenotype by altering the growth factor composition of the culture medium.

1.2 Co-culture models

In ICO models, only one cell type is represented: the cholangiocyte. However, *in vivo*, different liver cells work together to create and maintain a functional organ. Therefore, multiple cell types should be combined to create a culture model that resembles the native tissue. For liver models, hepatocytes, hepatic stellate cells (HSCs), Kupffer cells, and liver sinusoidal endothelial cells (LSECs) are promising co-culture candidates since they make up the majority of the liver tissue. When cells are cultured together in co-culture models, they will be able to communicate via direct and/or indirect cell-cell contact, allowing them to coordinate cell function. Numerous studies have shown the effectiveness of co-culture models in terms of improving the cell function of hepatobiliary cells. For example, hepatocyte function (assessed by measuring CYP activity and urea and albumin synthesis) was improved in co-culture models including non-parenchymal liver cells like HSCs, Kupffer cells, and LSECs. Additionally, non-liver-derived cells like 3T3 fibroblasts and human umbilical vein endothelial cells (HUVECs) also had the capacity to improve cell function [11,12]. In mono-cultures, factors such as culture surface, 2D or 3D growth, and medium composition are optimized for one specific cell type. The optimized culture environment often varies between different cell types. Therefore, one of the biggest challenges of designing a co-culture model is creating culture conditions that allow both cell types to maintain their phenotype and viability.

1.2.1 Mesenchymal stromal cells

Besides the aforementioned hepatobiliary cells, mesenchymal stromal cells (MSCs) can be considered as a potential co-culture candidate. This multipotent cell can be isolated from a large number of tissue sources, including the liver. The cells are plastic-adherent, express the surface molecules CD105, CD90 and CD73, lack the expression of CD45, CD34, CD14 or CD11b, CD79α or CD19 and HLA-DR, and are able to differentiate into osteoblasts, adipocytes, and chondrocytes *in vitro* [13,14]. Details on how MSCs function in the liver are still unknown. Nevertheless, research has shown that the presence of MSCs has a large influence on its environment. When placed in damaged tissue *in vivo*, MSCs will start to produce bioactive factors, regulate the local immune response, release anti-inflammatory factors, and activate site-specific stem cells [15–17]. Additionally, MSCs are able to downregulate the activation of HSCs in the liver. This is important because inflammation in the liver can induce the activation of HSCs with overproduction of ECM as a result. Continuous disbalance in the breakdown and production of ECM can cause an increase in stiffness, which impairs the functionality of the organ and can ultimately lead to end-stage liver failure. By downregulating the HSC activation, MSCs help to reduce fibrosis formation [18,19]. Currently, the potential of using MSC therapy to treat liver disease and improve liver transplantation is being studied in several clinical trials [20,21].

In co-culture models, MSCs can help improve the function and viability of other cell types. Studies have already demonstrated this effect in hepatocyte-MSC co-culture models [22]. Furthermore, in models combining MSCs with other (liver) cell types, spontaneous self-organization of organoid-like structures was observed. For instance, Takebe *et al.* showed that induced pluripotent stem cells (iPSCs), MSCs, and HUVECs self-organize into liver bud organoids [7]. Cordero-Espinoza *et al.* found that mitogens coming from SCA1+ mesenchymal cells help with ductal organoid formation and expansion, with MSC-organoid cell ratios as a regulatory factor [23]. Last, Ramachandran *et al.* combined hepatocytes, LSECs, and MSCs in Matrigel®, and saw self-organized organoid-like structures in 24 hours [24].

1.3 Extracellular matrix

The ECM is an important non-cellular component of the liver as it provides strength, shape and a surface for cells to adhere to. Cells react to the stiffness of the ECM, influencing cell phenotype and behavior, such as cell proliferation, migration, differentiation, and gene expression [25]. Besides structure, the ECM plays a role in cell communication since it contains proteins that function as signaling molecules and storage depots for growth factors and cytokines [26].

The majority of organoid culturing is performed in basement membrane extracts (BME) such as the commercially available Matrigel® (Corning) and BME (Cultrex). These hydrogels contain a mixture of ECM components derived from mouse tumor cells and are non-tissue-specific [27]. Moreover, these hydrogels are known to have large batch-to-batch variation and to stimulate cell proliferation rather than differentiation [28,29]. Therefore, the use of these hydrogels in hepatobiliary models might not be suitable. Alternatives include hydrogels or scaffolds composed of native tissue ECM, derived from decellularized livers. This native tissue ECM is organ-specific and therefore suitable to recreate the *in vivo* environment in liver models.

1.4 Aim of this research

Studies have shown that 3D culture, co-culture, and culturing on (liver-derived) ECM are successful methods to create models that resemble *in vivo* conditions. The goal of this project was to combine these methods to obtain a physiologically more relevant culture model. Human adult liver-derived ICOs, MSCs, and ECM were used since they represent components of the native liver microenvironment. Donor liver biopsies were collected to initiate ICOs [4] and to decellularize liver ECM [30]. Liver-derived MSCs (L-MSCs) were isolated from perfusion fluid of donor livers collected at liver transplantation procedures [31]. To assess the most optimal culture conditions, three experimental setups were tested. The effect of the L-MSC secretome on ICOs and differentiated ICO was analyzed by culturing ICOs in the presence of different types and concentrations of L-MSC-derived CM in BME (3.1.2). Thereafter, ICOs and L-MSCs were cultured together in different concentrations in BME in direct and indirect models, allowing the cells to interact and create direct cell-cell contact (3.1.3). For the last step of this study, ICOs and L-MSCs were cultured together in different ratios on liver-derived ECM scaffolds to assess recellularization capacity and to allow the cells to have cell-ECM interaction in addition to cell-cell interaction (3.2.2). The effect of the presence of L-MSCs on ICO culture was studied by analyzing the morphology of cells, visible interaction between cell types, and the expression of hepatocyte, cholangiocyte, MSC and proliferation markers.

2 Methods

2.1 Used cell types

2.1.1 Isolating and expanding of L-MSCs

L-MSCs were isolated from perfusates of donor livers collected during transplantation procedures. Donor livers were perfused with University of Wisconsin solution (UW) and human albumin solution. These solutions were collected after perfusion and contained many different cell types that can be isolated. Mononuclear cells, including L-MSCs, were collected from both types of perfusate using Ficoll® Paque Plus density gradient centrifugation (Appendix A). Because MSCs adhere to plastic surfaces, they can be separated from the non-attaching cells that are also present in the perfusates. Therefore, the cells were cultured in plastic flasks (2D), in Dulbecco's modified Eagle's medium/Ham's nutrient mixture F-12 (DMEM/F-12, 1:1 mixture), supplemented with 10% non-heat inactivated fetal calf serum (nhi-FCS), 100 IU/mL penicillin and 100 µg/mL streptomycin at 37°C, 5% CO_2. L-MSCs attached to the plastic at day 2, after which non-attaching cells were removed. The culture medium was refreshed every 2-3 days. L-MSCs were reseeded to larger surface areas when the culture reached 80% confluency, using Gibco™ Trypsin-EDTA (0.05%) (TE) and incubating at 37°C for 5 minutes. Cells were reseeded at a density of $15x10^3$ cells/cm^2.

2.1.2 ICO initiation and expansion

ICOs were established following the protocol of Huch *et al.* [4]. In short, liver biopsies obtained from healthy donor livers during liver transplantation were stored in UW. Biopsies were minced using scalpels and digested in 2.5 mg/ml Collagenase Type A (Sigma) for 20-30 minutes at 37°C. Subsequently, the suspension was strained (70um) and washed with cold Advanced DMEM/F12 ++++ (Adv. DMEM/F12 ++++, Appendix B). BME (Cultrex) was added to the cell pellet (the total quantity varied based upon the size of the cell pellet) and plated in 25 µl droplets in 24 or 48 well-plates. BME was solidified by placing the plate upside down (preventing cells from sinking to the bottom of the plate) for 30-60 minutes at 37°C. Start-up medium (Appendix B) was added after the BME was solidified. After 3 days, the start-up medium was replaced with expansion medium (EM, Appendix B). ICOs were passaged every 7-10 days with splitting ratios of 1:4 to 1:6, depending on the proliferation rate of the organoid cells. In the passaging process, the organoids were mechanically dissociated into small fragments by pipetting up and down with a 200 µl pipet. These fragments were reseeded in fresh 25 µl droplets of BME solution (70% BME, 30% Adv. DMEM/F12++++) on a 24 or 48 well-plate in EM at 37°C, 5% CO_2. The EM was refreshed every 2-3 days.

2.2 Preparation

2.2.1 Preparation of the CM

To model the effects of the L-MSC secretome on ICO growth, L-MSC-derived conditioned medium (CM) was created. Confluently grown T75 flasks with L-MSCs (N=1) were used to create the CM. The cells were weaned off serum by lowering the percentage of nhi-FCS with 2% per day for 5 days, adding fresh medium daily. Thereafter, the medium was replaced by 50 ml of Adv. DMEM/F12++++ to create the conditioned medium. The medium was kept with the L-MSCs for 1, 4, and 7 days, creating three different batches of CM, which will be referred to as CM1, CM4, and CM7. All the batches of CM were filtered with a 40 µm cell strainer before use to remove possible cellular debris.

2.2.2 Liver-derived ECM scaffolds

Liver-derived ECM scaffolds were obtained from decellularized donor livers and used in two co-culture setups. A human liver (N=1) was decellularized following the protocol by Willemse *et al.* [30]. A healthy human liver, deemed unsuitable for transplantation purposes, was used. This liver was rejected for transplantation by all Eurotransplant centers. The use of rejected human livers for research purposes was approved by the Erasmus MC medical ethics committee (MEC-2012-090). The liver was flushed with cold saline (0.9%) before storage at -20°C. After the liver was thawed, it was connected to the perfusion setup and perfused with dH2O at an average arterial pressure of 120 mmHG. The rotation of peristaltic pumps was adjusted to maintain this average pressure. The liver was perfused with 50L dH20, before being continuously perfused with 4% Triton-X-100 + 1%NH3 for 120 minutes. Afterward, the perfusate was refreshed with TX100 solution and changed to reperfusion. The liver was perfused for 120 minutes, and reperfusion cycles were repeated 9 times in total. After completion of the TX100 cycles, the liver was perfused with 100l dH2o and stored in 10L dH2O for two weeks. The dH2O was refreshed every other day. Finally, the liver was treated with DNase type 1 (5mg/L) in 0.9 NaCl + 100mM CaCl2 + 100mM MgCl2 solution. Complete decellularization was confirmed based upon DNA content and histology. The liver was stored at -20°C.

Round cylindrical biopsies were taken from the frozen liver using a dermal biopsy punch (6mm). The punches were cut using a cryotome (200um thickness) and the resulting discs were washed subsequentially 3x in 1X PBS, 3x in Adv. DMEM/F12++++ and 3x in Adv. DMEM/F12++++, supplemented with 10X primocin and 10x antibiotic-antimycotic. The last wash step was incubated overnight at 37°C. Afterward, the discs were washed 3x in Adv. DMEM/F12++++. Washed scaffolds were used directly or kept frozen until use.

2.2.3 Fluorescently labeled L-MSCs

To be able to track the L-MSCs in co-culture models, two different methods were used to create red fluorescent L-MSCs. Cells were genetically stable labeled with a red fluorescent (mCherry) protein by performing a lentiviral transduction. After 3 passages, mCherry positive cells were sorted using a FACS sorter (BD). As a second method, a red fluorescent lipophilic membrane dye (PKH26, Sigma-Aldrich) was used to stain the L-MSCs 1-3 hours prior to the start of the experiment.

2.2.4 L-MSC mono-culture in BME

Because L-MSCs are normally cultured in 2D culture flasks, a test mono-culture in BME was performed. L-MSCs were harvested from culture flasks using TE as described previously. Cell numbers were determined using a disposable plastic cell counter (Kova). The cells were added to 25 µl BME (100%) droplets and cultured in 48 well-plates in four different concentrations: 10,000, 7000, 3000, and 1000 cells/dome. Cells were cultured in Adv. DMEM/F12++++ and culture medium was refreshed every 2-3 days. After one week of culture, a LIVE/DEAD assay was performed.

2.2.5 L-MSCs mono-culture on ECM

Because L-MSCs are normally cultured in 2D culture flasks, a test mono-culture on ECM was performed. L-MSCs were harvested and counted as described previously. Frozen liver ECM scaffolds were thawed to room temperature, washed in PBS, and placed in a 48 well-plate in Adv. DMEM/F12++++. Right before adding cells to the scaffold, the medium was removed and the scaffold was made as dry as possible, without letting the scaffold dry out completely.

L-MSCs were cultured on liver-derived ECM in concentrations of around 10,000 cells/scaffold. A small droplet of Adv. DMEM/F12++++ that contained the cells was put on top of the scaffold and incubated for 2 hours at 37°C before adding the culture medium. Cells were cultured in Adv. DMEM/F12++++ and culture medium was refreshed every 2-3 days. After one week of culture, samples were stained with calcein-AM and DAPI and brightfield images were made.

2.3 Experiments

2.3.1 Cultivation of ICOs in the presence of L-MSC derived CM in BME

To model the effects of the L-MSC secretome on ICO growth and expression of hepatocyte, cholangiocyte, MSC and proliferation markers, ICOs were cultured in the presence of L-MSC-derived CM. Twelve different medium compositions were created by supplementing expansion medium (EM) and differentiation medium (DM) with 25% or 50% of one of the 3 different CM batches (CM1, CM4, and CM7). The concentrations of the EM and DM medium components (Appendix B) were kept constant between all medium compositions (except for Adv. DMEM/F12 ++++).

ICO cells (N=4, passage 5-7) were cultured in the 6 different medium mixtures of EM and CM, in 25 µl BME (100%) droplets in 48 well-plates for 3 passages. Organoids were passaged as described before with splitting ratios of 1:4 to 1:6, depending on the proliferation rate. As a second variant of the experiment, ICO cells (N=2) were differentiated towards hepatocytes. For this, organoids were cultured in the mixture of EM and CM for the first 2 passages. Three days after the second passage, 25 ng/ml BMP7 was added to the culture medium. From the second to the third passage, organoids were passaged with a split ratio of 1:1 and medium was changed to medium mixtures of DM and CM (the type and concentration of CM were kept constant).

The culture medium was refreshed every 2-3 days. At the end of the third passage, cells were fixed in 4% paraformaldehyde (PFA) for 10 minutes for histological analysis. Additionally, the cells (mixture of 4 wells) were lysed in Qiazol lysis reagent (Qiagen) and stored at -80°C for quantitative polymerase chain reaction (qPCR) analysis. A schematic overview of the experiments can be found in Appendix C.

2.3.2 Direct and indirect co-cultivation of ICOs and L-MSCs in BME

ICOs and L-MSCs were cultured together in different concentrations in BME, allowing the cells to interact and create direct cell-cell contact. ICO cells (passage 5-10) were harvested from the BME by using cold Adv. DMEM/F12++++ and mechanically breaking down the BME structure into small fragments. After removal of the BME, TE was added to the ICO cell pallet and incubated at 37°C for 30-60 minutes until a single cell suspension had formed. Cell numbers were determined using a disposable plastic cell counter (Kova). Red fluorescent L-MSCs (passage 13), created with transduction of a vector containing the mCherry-gene, were harvested from culture flasks and cell numbers were determined as described previously.

ICOs and L-MSCs were cultured in direct and indirect BME co-culture models. Cells were cultured in EM in 48 well-plates for 3 weeks (without passaging). For the direct co-culture (ICO N=3, L-MSC N=1), a mixture of both cell types was added directly into the BME (100%), and the medium was added after solidification of the BME. For the indirect co-culture (ICO N=2, L-MSC N=1), ICO cells were added to the BME, and L-MSCs were added in the medium after solidification of the BME, allowing the cells to adhere on the plastic surface of the well-plate and on top of the BME. Cells were seeded in six different ICO:L-MSC ratios: 1:0, 1:1, 10:1, 100:1, 1:5 and 0:1. The total number of cells per BME dome/well was around 5000 cells for all conditions. The culture medium was refreshed every 2-3 days. On day 21, cells were fixed in 4% PFA for 10 minutes for histological analysis. Cells (mixture of 4 wells) were lysed in Qiazol and stored at -80°C for the qPCR analysis. A schematic overview of the experiments can be found in Appendix C.

2.3.3 Direct and MSC-first direct co-culture on ECM

ICOs and L-MSCs were cultured together on ECM scaffolds, allowing the cells to have interaction with liver-derived ECM in addition to cell-cell interaction. ICOs (passage 5-10) and red fluorescent L-MSCs (passage 6 and 7), created by adding the red fluorescent lipophilic membrane dye, were

harvested and counted as described previously. Frozen liver ECM scaffolds were prepared for the experiment as described before in 2.2.5.

ICOs (N=4) and L-MSCs (N=2) were co-cultured on decellularized liver ECM in a direct and MSC-first direct co-culture model in EM for 3 weeks (no passaging). For the direct co-culture, both cell types were mixed and placed simultaneously on top of the liver ECM. Cells were seeded in 5 ICO:L-MSC ratios: 1:0, 1:1, 10:1, 100:1 and 0:1. For the MSC-first direct co-culture, L-MSCs were pre-cultured for 3 days, adding L-MSCs on day 1 and ICOs on day 4. Two ICO:L-MSC ratios were initiated: 1:1 and 10:1. The cells were added to a small droplet of Adv. DMEM/F12++++, placed on top of the scaffold and incubated for 2 hours at 37°C before the culture medium was added. The total number of seeded cells was constant between conditions at around 25,000 cells per scaffold. ICO (1:0) and ICO-L-MSC (ratio 1:1) cultures in BME (5000 cells per dome) were used as extra control.

The culture medium was refreshed every 2-3 days. Around 80% of the old medium was removed and supplemented with fresh medium to prevent the scaffold from drying out during the medium changing process. At the end of the third week, cells were fixed in 4% PFA for 20 minutes for histological analysis. Cells (mixture of 4 wells) were lysed in Qiazol and stored at -80°C for the qPCR analysis. A schematic overview of the experiments can be found in Appendix C.

2.4 Analysis

2.4.1 Cell viability

For LIVE/DEAD assessments, the culture medium was supplemented with 100 µg/ml Hoechst, 12.5 µg/ml propidium iodide (PI), and 0.5 µM calcein-AM, and the cultures were incubated for one hour at 37°C in the dark. Hoechst was used to locate cell nuclei, PI (red) was used to locate dead cells and calcein (green) was used to identify living cells. Pictures were made with an EVOS® FL Cell Imaging System or a Leica SP5 confocal microscope.

2.4.2 Histology

Histology was performed to analyze the general morphology of cells. Formalin-fixed (4%) samples were embedded in agarose, followed by paraffin embedding. The samples were cut in sections with a thickness of 4 µm with a microtome. The sections were placed on glass microscope slides and stained with hematoxylin and eosin (H&E). For this, sections were deparaffinized by consecutively incubating the section in two changes of xylene and decreasing concentrations of EtOH (100%, 95%, and 70%) for 5 minutes each. Then, the sections were stained by putting them in filtered hematoxylin for 1 minute and in eosin for 10 minutes. Subsequentially, the sections were dehydrated by following the deparaffinization protocol in reversed order. Sections were mounted with Pertex. Pictures were made using a Zeiss Axiokop 20 microscope and captured with a Nikon DS-U1 camera.

2.4.3 Immunohistochemistry

Immunohistochemistry was performed on formalin-fixed (4%) samples and formalin-fixed (4%), paraffin-embedded and sectioned (4 µm) samples to assess the expression of cholangiocyte markers cytokeratin (CK) 7 and 19.

Formalin-fixed samples were used for whole-mount staining. The samples were incubated at room temperature in a 1x PBS 0.1% Triton-X-100 mixture for 20 minutes, followed by incubation in a 1x PBS 5% serum mixture for 1 hour. The primary antibody CK7 (DAKO, Mouse anti-human, 1:100) was added to samples and incubated overnight at 4°C. The primary antibody was not added to the negative control samples. After washing, the secondary antibody (Alexa Fluor 555, goat anti-mouse, 1:100) was incubated at room temperature for 1 hour. Additionally, the samples were stained with Phalloidin Alexa Fluor 488 (actin staining) and DAPI (DNA staining). Imaging was done

with a Leica 20X water dipping lens on a Leica DM6000 CFS microscope with a LEICA TCS SP5 II confocal system. Images were processed using ImageJ to obtain maximum intensity projection images.

The sectioned samples were deparaffinized as described previously and antigen retrieval was performed in a TRIS-EDTA buffer (pH 8-9) at around 90 °C for 10 minutes. Primary antibodies CK7 (Mouse anti-human, 1:100) and CK19 (Mouse anti-human, 1:100) were incubated overnight at 4°C. After washing of the sections, secondary antibodies (goat anti-mouse, 1:100) were incubated for 1 hour at room temperature. DAPI was added before covering the sections with a glass slip. Sections were imaged with a Leica SP5 confocal microscope. Images were processed using ImageJ software.

2.4.4 RNA isolation and RT-PCR

Qiazol lysed samples were used to extract RNA with the NucleoSpin RNA isolation kit (Machery Nagel), following the manufacturer's instructions. The ECM co-culture samples were homogenized with a TissueRuptor (Qiagen) before RNA extraction. The RNA content and purity were measured with the NanoDrop spectrophotometer. Complementary DNA (cDNA, 400 ng) was made using 5x PrimeScript RT Master Mix and a thermal cycler. cDNA (4 ng/µl) was mixed with SYBR select master mix and gene-specific primers (GAPDH, HPRT-1, B2M, LGR5, CK7, CK19, EPCAM, KI67, Vimentin, Albumin, CYP3A4, CD105 and CD90, Appendix D) and the gene expression was measured with a StepOnePlus real-time PCR System (Applied Biosystems). Gene expression levels are displayed as $2^{-\Delta CT}$ and normalized to the geometrical average of the housekeeper genes GAPDH, HPRT-1, and B2M. The data was analyzed by performing One-way ANOVA and matching multiple comparison tests with GraphPad Prism software (version 8.0). A *p*-value lower than 0.05 was considered statistically significant.

3 Results

3.1 Cultures in BME

3.1.1 Culture of ICOs and L-MSCs separately

Mono-cultures of ICOs and L-MSCs give insight into normal growth patterns and form a baseline for co-culture studies. This section focuses on morphology, growth patterns, and viability of ICOs and L-MSCs cultured in BME.

3.1.1.1 ICO morphology and donor variation

ICOs were cultured in BME in standard expansion medium (EM, Appendix B) [4]. After seeding, the organoid cells formed hollow spheroids that grew in size over the culture period of 1-3 weeks. Between donors (N=9), a variation in the size and density of the organoids was observed. Figure 1A-D shows this variation in representable examples of four different donor lines. Moreover, differences in the growth rate were observed between donor lines. Figure 1E illustrates three donor lines from week 2 to 3 of culture, showing clear differences in the degree of organoid growth. In some cultures, more 2D growth (visible as monolayers of cells on the plastic well-plate surface) was observed (Figure 1A). This can be caused by a lower stiffness of the BME, which can occur if the seeding BME-medium ratio is too low, or when cells are cultured in the same BME dome for prolonged periods of time.

Because culture conditions were kept constant, variations can be explained by donor-donor variances. Large variations in organoid number and size caused by differences in proliferation rate can be minimized by adjusting the split ratio and frequency of splitting.

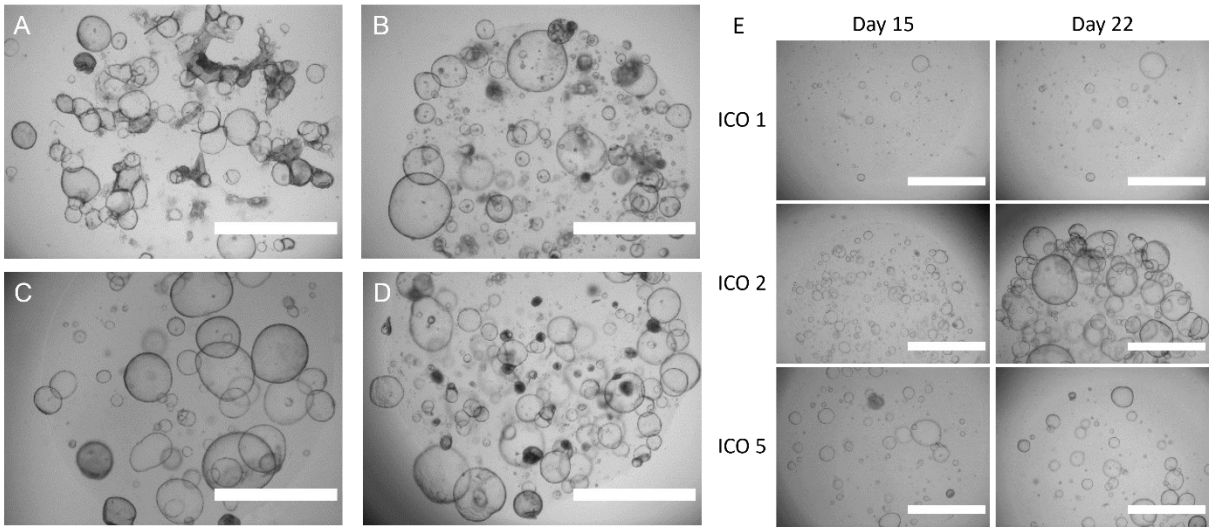

Figure 1. Brightfield images showing donor-donor variances of ICO culture. The scale bar represents 2000 µm. Images of four representable donor lines show variances in organoid size and denseness after one week of culture (A-D). Patches of cells on the plastic well-plate indicate 2D growth (A). Dense organoids are recognizable by their darker color and lack of transparency. Images of 3 representable donor lines of week 2 and 3 of culture show differences in ICO proliferation rate (E). Initial seeding densities of all three ICO lines were constant at around 5000 cells per done (E).

3.1.1.2 Morphology and viability of L-MSCs

Conventionally, MSCs are expanded on a plastic surface in 2D, using an MSC specific medium (Appendix B). The MSCs form a confluent layer of fibroblast-like spindle-shaped cells (see Figure 2A). To test the potential of L-MSCs to grow in ICO conditions and ICO basal medium (Adv. DMEM/F12++++), L-MSCs were seeded in different concentrations in BME and cultured for a period of one week. Cells grew inside the BME and migrated towards the plastic surface of the well underneath and around the BME. The L-MSCs inside the BME were either long and elongated cells, or smaller and round cells, as can be seen in the calcein staining of Figure 2B and C. The proportion of the small, round morphology was higher in conditions with lower concentrations of L-MSCs (3000 and 1000 cells/dome). Cells growing on the plastic surface had the classic fibroblast-like morphology and seemed to be slightly wider than the thin, elongated cells inside the BME. LIVE/DEAD staining (see Figure 2B and C) was performed after one week of culture. Live cells are green (calcein), and dead cells are red (PI). In all different L-MSC concentrations, cells remained viable after one week of culture (cell death <5%). This indicated that it is possible to grow viable L-MSCs in ICO conditions and basal medium.

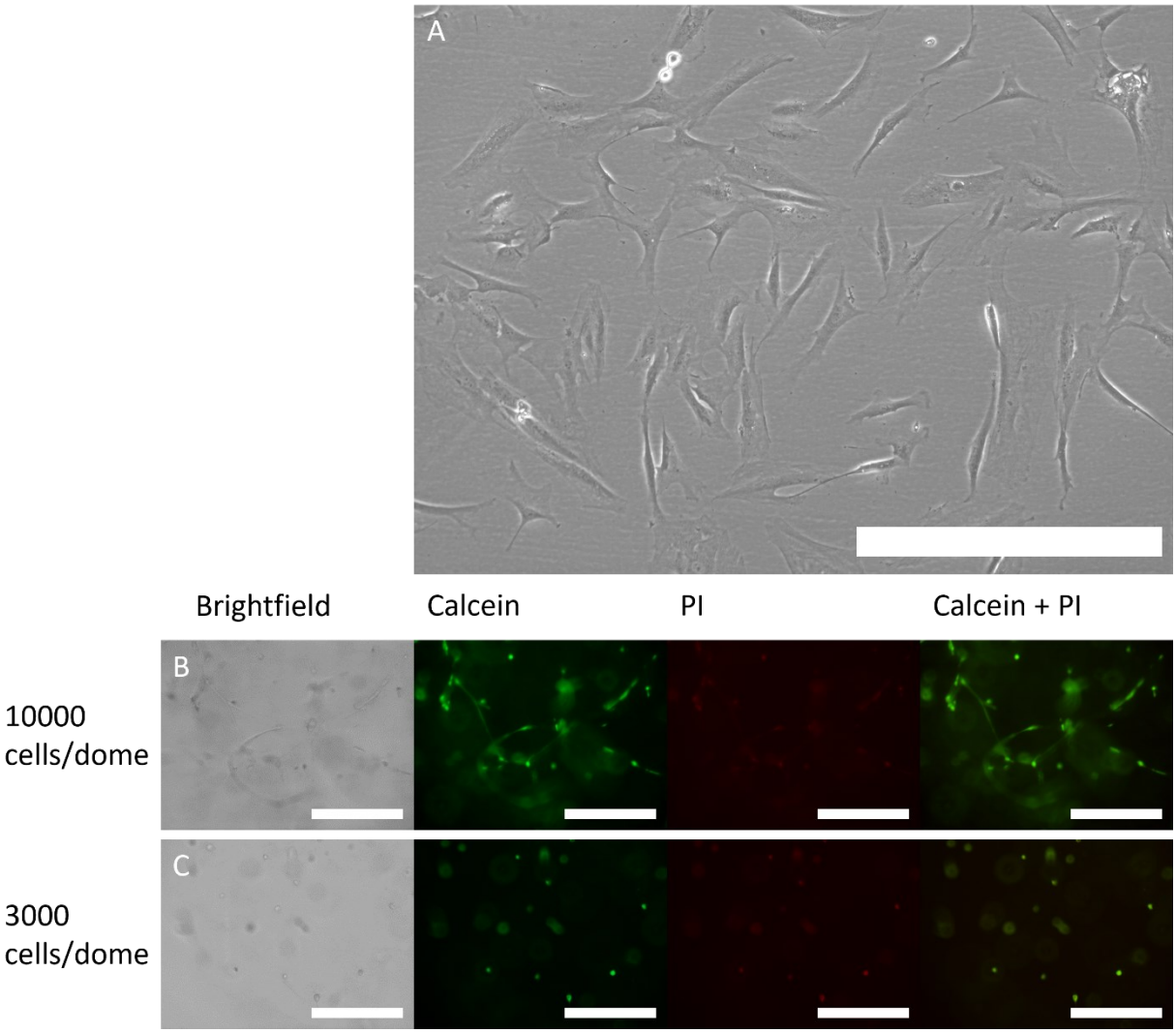

Figure 2. L-MSCs cultured in 2D on a plastic surface had spindle-shaped, fibroblast-like morphology (A). A LIVE/DEAD assay showed little cell death after a week of L-MSC culture in BME (B, C). Scale bars represent 1000 (A) and 400 (B, C) µm. The red PI signal overlaps with the green calcein signal and is not specifically located at the nuclei of the cells, suggesting crosstalk of the channels.

3.1.2 Cultivation of ICOs in the presence of L-MSC derived conditioned medium

CM can be a rich source of biomolecules secreted by L-MSCs, like soluble proteins, lipids, extracellular vesicles, and other compounds that aid in tissue repair and regeneration [32–34]. It can be used to relatively easily create an indirect co-culture model since the two cell types are cultured in their own “optimized” environment, and CM of the first cell type can simply be added to the culture medium of the second cell type. Therefore, the first step of this study was to culture ICOs in the presence of different types and concentrations of L-MSC-derived CM to assess the effect of the L-MSC secretome on ICO growth and the expression of hepatocyte, cholangiocyte, MSC and proliferation markers. In this section, the main results will be discussed. An overview of brightfield images of all culture conditions can be found in Appendix E.

3.1.2.1 Effect of CM on morphology and growth pattern of EM ICOs

In general, the EM ICOs were able to expand in the different types and concentrations of CM to a similar degree as the control condition (0% CM). The time between passages and split ratio were constant between all conditions (including the control condition), ranging from 7 to 10 days and 1:4 and 1:6 depending on the donor line. However, variation in the number of organoids, organoid size, organoid density, and 2D growth was observed between the different conditions (illustrated with brightfield images in Appendix E). For example, for donor line 4, the control and EM+CM1 conditions contained noticeably more organoids than the EM+CM4 and EM+CM7 conditions. Although variations were observed in all four donor lines, especially in lines 1 and 4, no clear repeating trends were observed. Besides the presence of the CM, natural culture variation could explain differences between conditions.

The viability of the ICOs cultured in EM+CM was analyzed using a LIVE/DEAD assay, performed at the end of the third passage. For all EM+CM conditions, low numbers of dead cells (0-10 cells per organoid) were detected. The control condition revealed an ICO with the highest number of dead cells (see Figure 3).

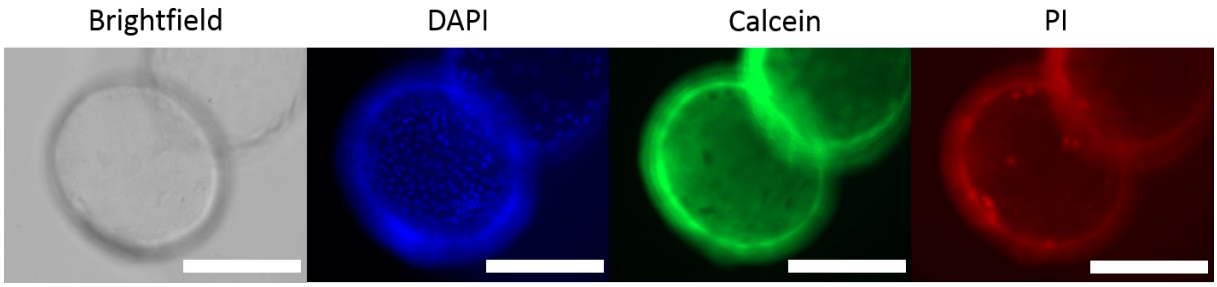

Figure 3. LIVE/DEAD assay of the control condition (0% CM) of the EM+CM experiment revealed a small number of dead cells. Dead cells are characterized by amplified PI signal and a lack of Calcein signal. Scale bars represent 300 µm.

3.1.2.2 Effect of the CM on gene expression of EM ICOs

The gene expression of hepatocyte (Albumin and CYP3A4), cholangiocyte (EPCAM, CK7, and CK19), MSC (CD90, CD105, and Vimentin), proliferation (KI-67), and stem cell (Lgr5) markers was measured in all EM+CM (N=3) conditions by performing a quantitative PCR analysis. The results are summarized in Figure 4. In general, no statistically significant differences were found between the different conditions.

Compared to the control (0% CM) condition, mean KI-67 expression was lower in all EM+CM conditions (on average 2.2-fold, SD:±1.1), suggesting that cell proliferation is downregulated by the presence of the CM. The mean EPCAM expression followed a similar pattern (on average a 1.5-fold decrease in EM+CM conditions, SD:±0.15). Conversely, the mean expression of Lgr5 and Vimentin was higher in the EM+CM conditions (on average 1.8-fold, SD:±0.45, and 4.2-fold, SD:±0.98). The mean expression of cholangiocyte markers CK7 and CK19 varied between

conditions, showing both upregulation and downregulation compared to the control condition. Expression of MSC and hepatocyte markers was low in the samples. CD90 and CD105 expression was undetectable for all conditions, and Albumin and CYP3A4 expression was undetectable for a number of samples. CM1 in a 25% concentration seemed to increase CYP3A4 expression, whilst other CM types and concentrations decreased expression. Overall, no large effects of CM on gene expression were observed in these samples.

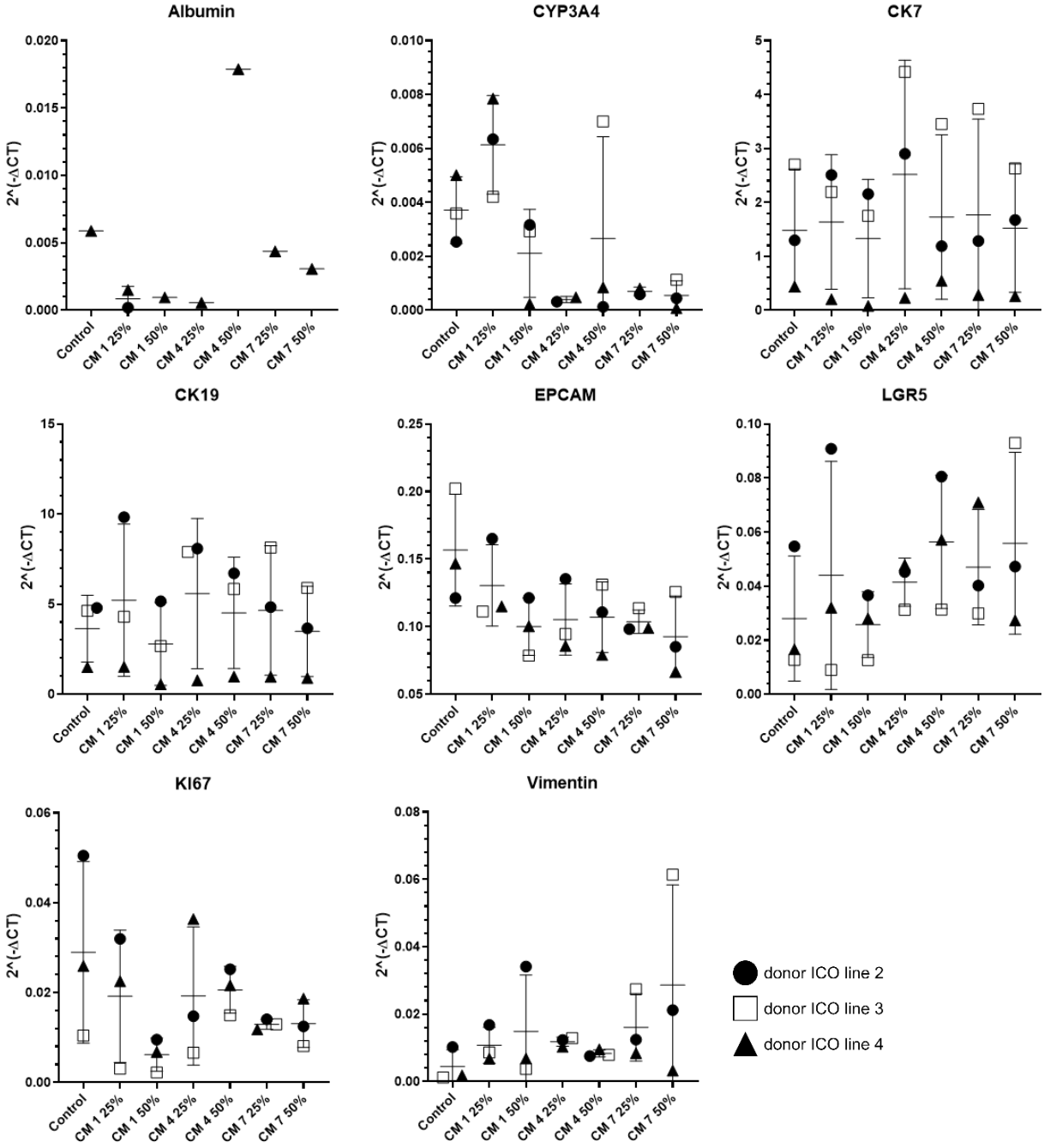

Figure 4. RNA expression data of EM ICOs cultured with different types and concentrations of CM. Expression of hepatocyte (Albumin and CYP3A4), cholangiocyte (CK7, CK19, and EPCAM), stem cell (Lgr5), proliferation (KI-67), and MSC (Vimentin, CD90, and CD105) markers are shown if detectable. Data is displayed as $2^{-\Delta Ct}$. No statistically significant differences were found between the different conditions. The mean KI-67 and EPCAM expression were downregulated in EM+CM conditions. Mean LGR5 and Vimentin expression was upregulated in EM+CM conditions. CK7 and CK19 expression were both up- and downregulated between the different conditions. Expression of MSC markers CD90 and CD105 were undetectable. Hepatocyte markers Albumin and CYP3A4 were undetectable for a number of samples.

3.1.2.3 *Effect of the CM on morphology and growth pattern of differentiated ICOs*

ICOs have the potential to differentiate towards hepatocytes by changing the medium composition. Cultured in differentiation medium (DM), the cells will start to express hepatocyte-specific markers and morphology [4]. Previous research has shown that hepatocyte function and viability can be improved by the presence of MSCs in co-culture models [22]. The efficacy of L-MSC-derived CM to enhance the expression of hepatocyte markers in differentiated organoids was investigated by culturing ICOs in DM+CM.

After switching from EM+CM to DM+CM after the second passage, the morphology and proliferation rate of ICOs changed significantly. The organoids became smaller and denser, as can be seen in Figure 5. Additionally, the proliferation rate was lower in DM than in EM cultures. The number of organoids per dome in the second passage (EM) was roughly comparable to the third passage of both EM and DM cultures. Because the splitting ratio was 1:1 for DM ICOs, and 1:4 for EM ICOs, it can be concluded that the proliferation rate changed. Small variations in organoid density were observed between the different DM+CM conditions (see Figure 5). For example, the CM4 50% conditions (Figure 5C, F, and Appendix E) contained less dense organoids, characterized by defined dark outlines and more transparent middles, compared to other conditions like the CM1 25% cultures.

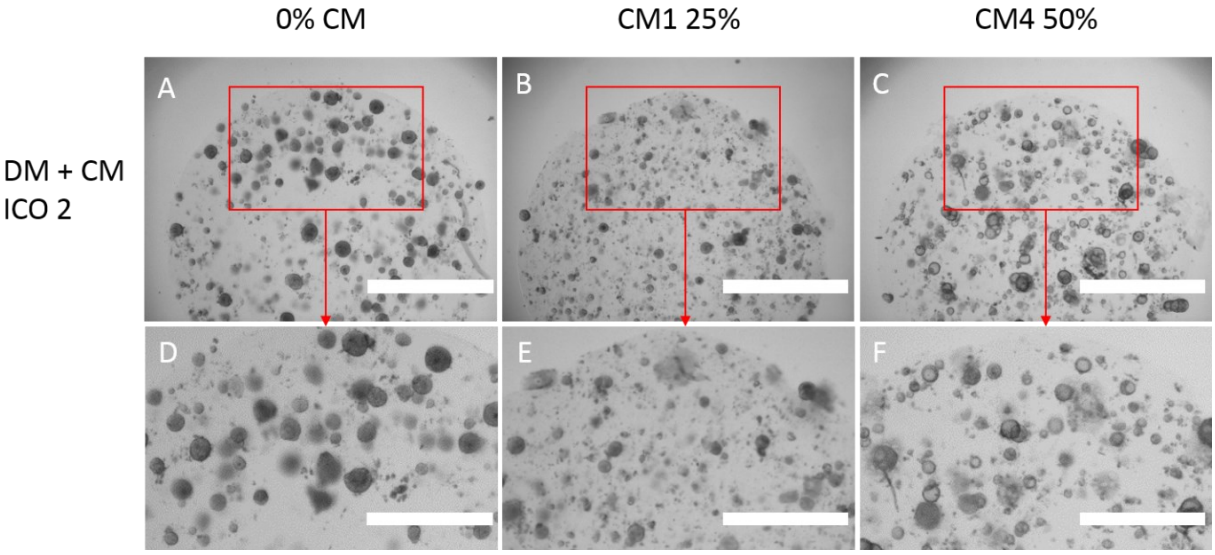

Figure 5. Brightfield images of the DM+CM cultures at the end of the third passage show variation in organoid density. In this image, ICO 2 is showed as a representable example. Scale bar represents 2000 µm (A-C) and 1000 µm (D-F). The CM4 50% condition (C, F) contained less dense organoids, with defined dark outlines and lighter middles, compared to other conditions like the control and CM1 25% condition. The CM4 50% condition of the other donor line also showed less dense organoids, as can be seen in Appendix E.

3.1.2.4 *Effect of CM on gene expression of differentiated ICOs*

The gene expression levels of one donor ICO line cultured in EM+CM and DM+CM are summarized in Figure 6. Contrary to EM cultures, Albumin and CYP3A4 expression was detectable in all samples with differentiated ICOs. The expression of Albumin and CYP3A4 in the DM+CM conditions was notably lower (on average 95-fold, SD:±5 and 500-fold, SD:±1000) than in the DM control condition (0% CM). This indicates that the presence of CM considerably downregulates the expression of hepatocyte markers. Additionally, the downregulating effect on CYP3A4 expression was stronger in 50% CM concentrations than paired 25% CM concentrations. Compared to EM cultures, KI-67, Lgr5, CK7, and CK19 expression dropped and Vimentin expression was higher in DM conditions. KI-67 and Lgr5 expression remained stable between different DM conditions. CK7 and Vimentin expression was upregulated (on average 1.5-fold, SD:±0.25 and 4.2-fold, SD:±2.0) and CK19 was downregulated (on average 1.5-fold, SD:±0.26) in DM+CM conditions compared to the DM control. Research by Akbari *et al.* showed that switching from EM to DM downregulates the

expression of EPCAM in their organoids [35]. In our model, this effect was not observed, and mean EPCAM expression was higher in DM organoids. CD90 expression was undetectable for all samples, and CD105 expression was low and undetectable for several samples.

In conclusion, the gene expression levels showed that the presence of CM did not upregulate but downregulated the expression of hepatocyte markers in differentiated ICOs. Additionally, the presence of CM did not clearly downregulate the expression of cholangiocyte markers since CK7 expression was upregulated in DM+CM conditions. Therefore, the differentiated ICOs were not included in the next co-culture experiments.

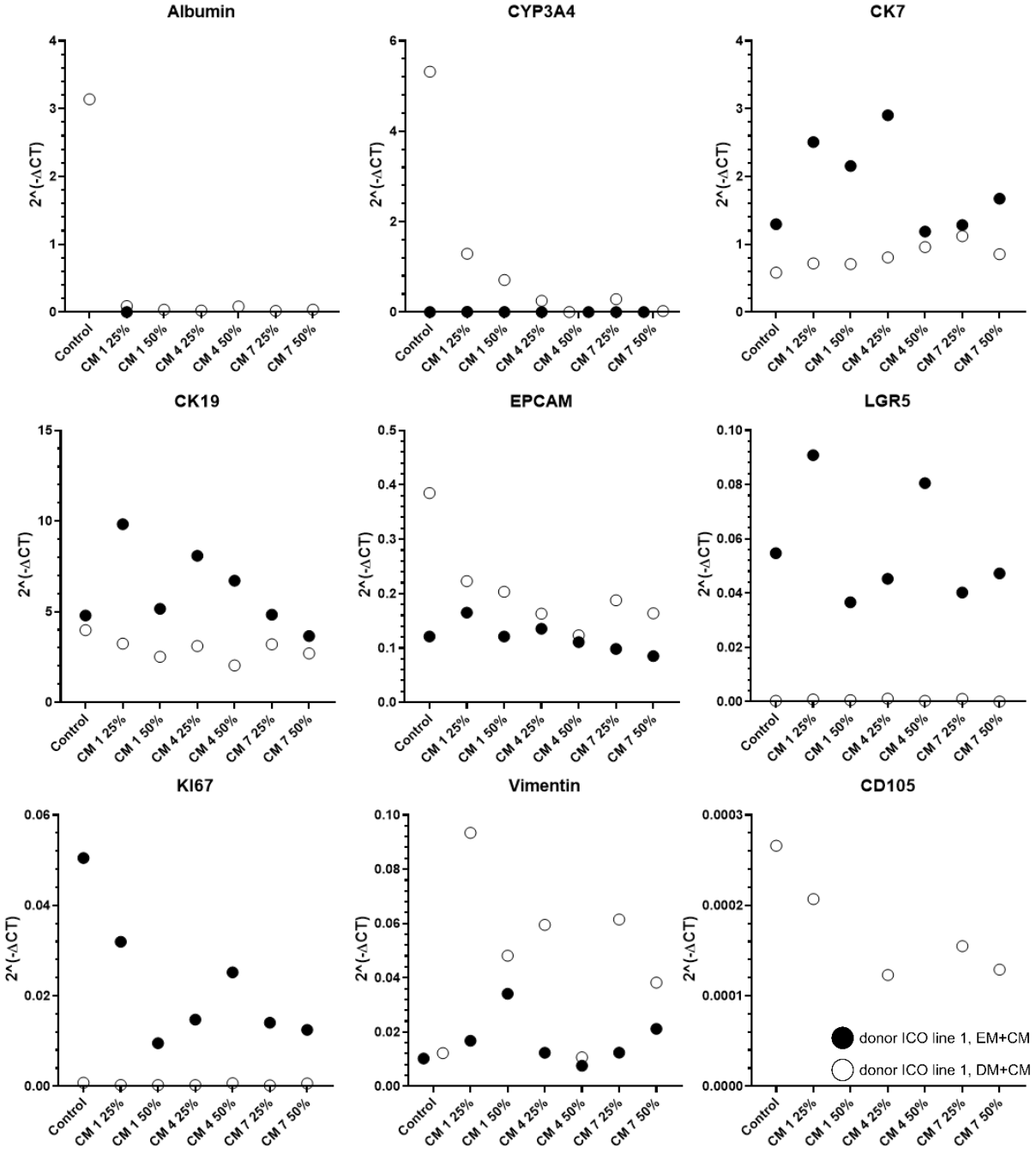

Figure 6. RNA expression data of EM versus DM ICOs, cultured with different types and concentrations of CM. Expression of hepatocyte (Albumin and CYP3A4), cholangiocyte (CK7, CK19, and EPCAM), stem cell (Lgr5), proliferation (KI-67), and MSC (Vimentin, CD90, and CD105) markers are shown if detectable. Data is displayed as $2^{-\Delta Ct}$. No statistically significant differences were found between the different conditions. Albumin and CYP3A4 expression were downregulated in DM+CM cultures compared to the DM control. Compared to EM ICOs, KI-67, Lgr5, CK7, and CK19 expression dropped and Vimentin and EPCAM expression increased. KI-67 and Lgr5 expression remained stable between different DM conditions. The CK7 and Vimentin expression were upregulated and CK19 was downregulated in DM+CM conditions. CD90 and CD105 expression were low or undetectable.

3.1.3 Direct and indirect co-cultivation of ICOs and L-MSCs

As the effect of the CM on ICO growth and gene expression seemed to be limited, more complex co-culture models were created and studied. ICOs and L-MSCs were cultured together in different concentrations in BME, allowing the cells to interact and create direct cell-cell contact. Two different variations of BME co-cultures were created: a direct and an indirect co-culture model. In this section, the main results will be discussed. An overview of brightfield images of all culture conditions can be found in Appendix F.

3.1.3.1 Effect of L-MSCs on morphology and growth pattern of ICOs

In general, the presence of the L-MSCs had no visible impact on ICO morphology and growth patterns in all culture conditions. ICOs were able to expand in the presence of L-MSCs in both the direct and indirect co-cultures for a culture period of three weeks. On day 1, single cells were observed. After 7 days of culture, small organoids had formed. The number and size of these organoids continued to increase in week 2 and 3. Donor variations (as described before in 3.1.1.1), e.g. differences in proliferation rate, were visible between donor lines. Although ICO morphology was consistent between all conditions per donor line, the total number of organoids in the ICO:L-MSC 1:5 cultures was significantly lower than in cultures of other conditions (see Appendix F). This difference can be explained by the lower seeding density of ICO cells for this condition, as the total ICO + L-MSC number was kept constant at around 5000 cells/dome for all conditions.

3.1.3.2 Direct cell-cell contact of ICOs and L-MSCs

In both the direct and indirect BME co-cultures, the majority of the L-MSCs did not have direct cell-cell contact with ICOs or each other. Nevertheless, instances of direct cell-cell contact were observed in the direct co-culture, especially in the conditions with higher concentrations of L-MSCs (in the range of 0-2 instances per dome). In the indirect co-cultures, most L-MSCs grew on the plastic surface and on top of the BME dome. Several L-MSCs migrated towards and inside the BME, growing in close proximity to ICOs. This phenomenon was observed mostly in the 1:1 and 1:5 ICO:L-MSC conditions of cultures of donor ICO line 1 (in the range of 0-3 instances per dome). In a number of cases, it was difficult to detect if the L-MSCs had truly penetrated the BME or were growing on top of the BME near an organoid. Nonetheless, multiple examples of L-MSCs in close proximity to organoids were observed, as can be seen in Figure 7A-H. The cells were red fluorescent in confocal images, confirming that they were L-MSCs (see Figure 7I-K). The red signal was detected mostly in the thicker parts of the L-MSCs. Additionally, calcein staining indicated that ICOs and L-MSCs remained viable for three weeks in each other's presence.

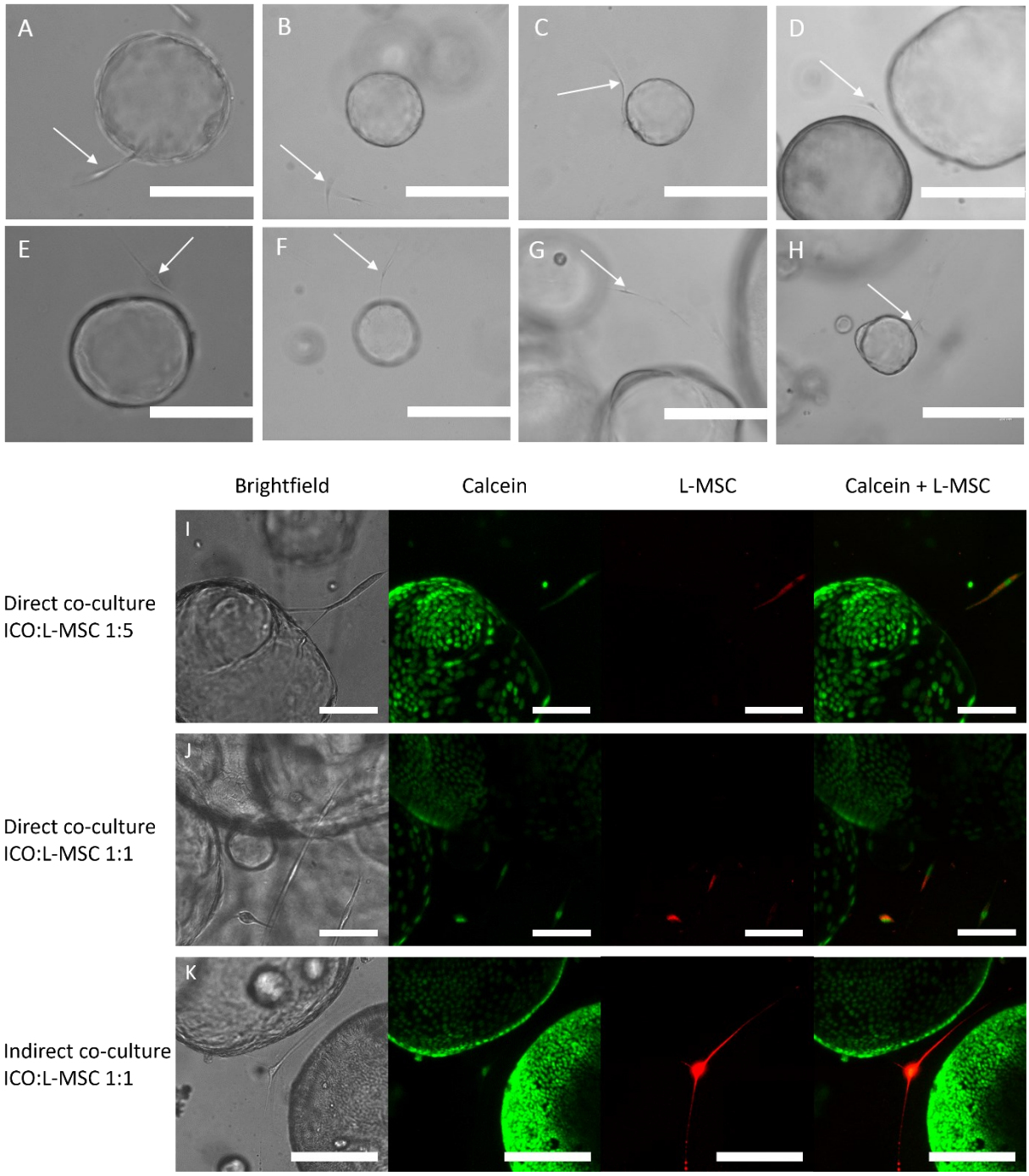

Figure 7. Brightfield images of the ICO:L-MSC 1:1 or 1:5 condition after 3 weeks of indirect co-culture in BME (A-H) show MSC-like structures (see arrows) in close proximity to organoids. Images A-F are of donor ICO line 1, and images G and H are of donor ICO line 2. Confocal images show three examples of ICOs and L-MSCs in close proximity in BME co-culture models (I-K). L-MSCs are red fluorescent. Calcein staining showed that cells remained viable after three weeks of culture. Scale bars represent 400 µm (A-H) and 100 µm (I-K).

3.1.3.3 *CK7 expression*

To assess CK7 expression, immunohistochemical analysis was performed on sections of the BME co-culture samples. In all direct and indirect co-culture conditions, ICOs cells were CK7 positive, indicating that the presence of L-MSCs did not influence the CK7 expression of these cells. Figure 8 shows representable examples of the stainings. The monolayer of organoid cells is revealed by the green CK7 signal.

Studies have shown that MSCs are CK7 negative [36]. A visible cell nucleus in combination with a lack of CK7 expression could indicate the presence of an L-MSC. Although hardly detected, Figure 8 shows two examples of CK7 negative cells that are not part of an organoid, indicating a potential L-MSC.

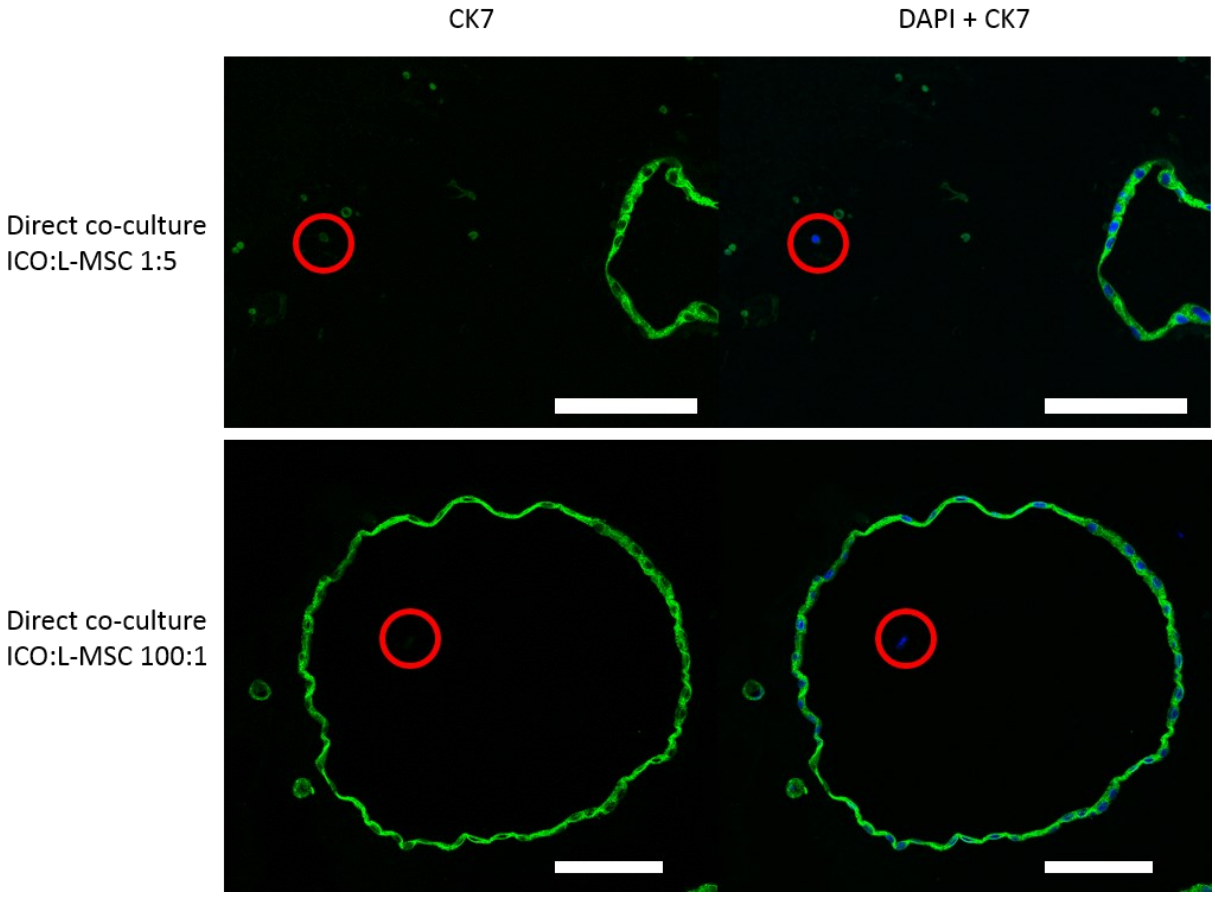

Figure 8. Confocal images of sections of the 1:5 and 100:1 condition of the direct co-culture in BME. Scale bars represent 100 µm. Sections were stained for the cholangiocyte marker CK7 and nuclei were made visible using DAPI. Monolayers of ICO cells were CK7 positive. Cells in the red circles, the potential L-MSCs, were CK7 negative and were not part of the ICO monolayer.

3.1.3.4 Gene expression

Gene expression of all direct (N=3) and indirect (N=2) co-culture conditions was measured. The data is summarized in Figure 9 and Figure 10. Unfortunately, RNA extraction of the 0:1 condition resulted in low concentrations (≤ 10 ng/µL) with questionable purity. Results are included but should not be used to draw definite conclusions. In general, no statistically significant differences were found between the direct co-culture conditions. Additionally, no major differences in gene expression were observed between the direct and indirect co-culture samples.

The expression of the hepatocyte markers Albumin and CYP3A4 was low and undetectable for a number of direct and indirect co-culture conditions. Contrary to CM cultures, expression of MSC markers CD90 and CD105 was detectable in both the direct and indirect co-cultures, although not for every condition. The expression was highest in the L-MSC-only condition and decreased as the L-MSC concentration went down. In ICO-only conditions, the expression was hardly or not detectable. Therefore, CD90 and CD105 expression can most probably be ascribed to L-MSCs derived RNA. Expression of the third MSC marker Vimentin followed a similar trend. The mean expression was on average 1.8-fold and 6.0-fold higher in the 1:1 and 1:5 direct co-culture conditions than in the ICO-only condition. The mean expression of cholangiocyte markers CK7, CK19, and EPCAM in co-culture conditions varied. Both up- and downregulation was observed in co-culture conditions compared to the ICO-only condition. The mean expression of stem cell marker Lgr5 was slightly lower in the presence of L-MSCs in direct co-culture conditions (on average 1.3-fold, SD:±0.02) than in the ICO-only condition. This trend is opposite to the upregulating effect of CM observed in EM+CM cultures. For the indirect co-cultures, the Lgr5 expression was stable between conditions. Expression of the proliferation marker KI-67 was highest in the 1:5 conditions in both the direct and indirect co-cultures. In other co-culture conditions, the expression was lower than in the control condition. This could indicate that there is a turning point between the 1:1 and 1:5 ratio where the presence of L-MSC starts to have an upregulating effect on cell proliferation.

Overall, variation in gene expression levels between conditions and direct and indirect samples was observed. However, these variations were generally small (with exception of MSC markers in the L-MSC-only condition) and revealed no clear effects of L-MSC on the gene expression.

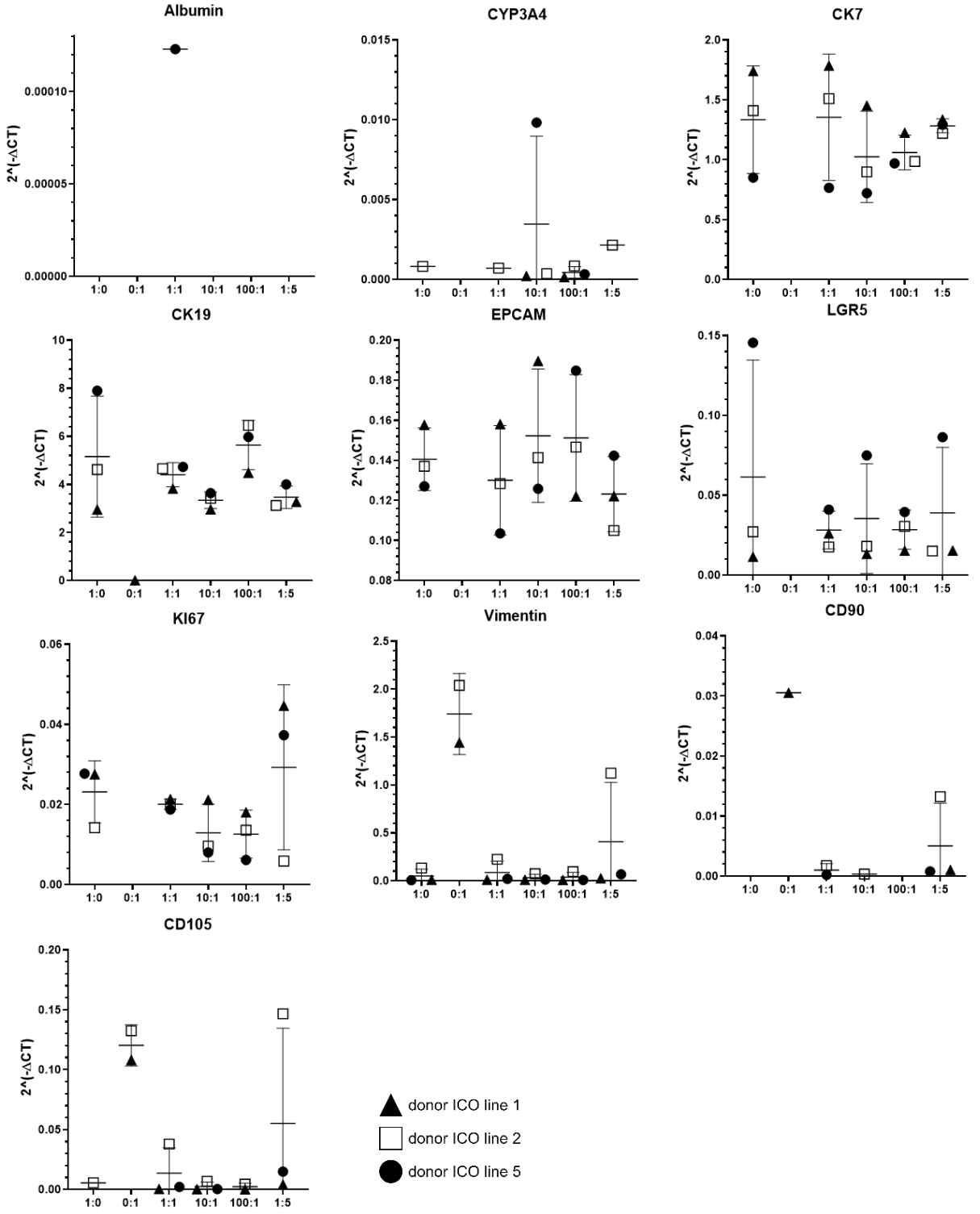

Figure 9. RNA expression data of the direct co-culture in BME (ICO:L-MSC). Expression of hepatocyte (Albumin and CYP3A4), cholangiocyte (CK7, CK19, and EPCAM), stem cell (Lgr5), proliferation (KI-67), and MSC (Vimentin, CD90, and CD105) markers are shown if detectable. Data is displayed as $2^{-\Delta Ct}$. Albumin and CYP3A4 expression are low or undetectable. The mean expression of MSC markers CD90, CD105, and Vimentin are highest in conditions with relatively high L-MSC concentrations. The mean expression of cholangiocyte markers CK7, CK19, and EPCAM in co-culture conditions varied. Both up- and downregulation was observed in co-culture conditions compared to the ICO-only condition. Lgr5 expression in the direct co-culture conditions was slightly lower in the presence of L-MSCs. The mean KI-67 expression is highest in the 1:5 condition.

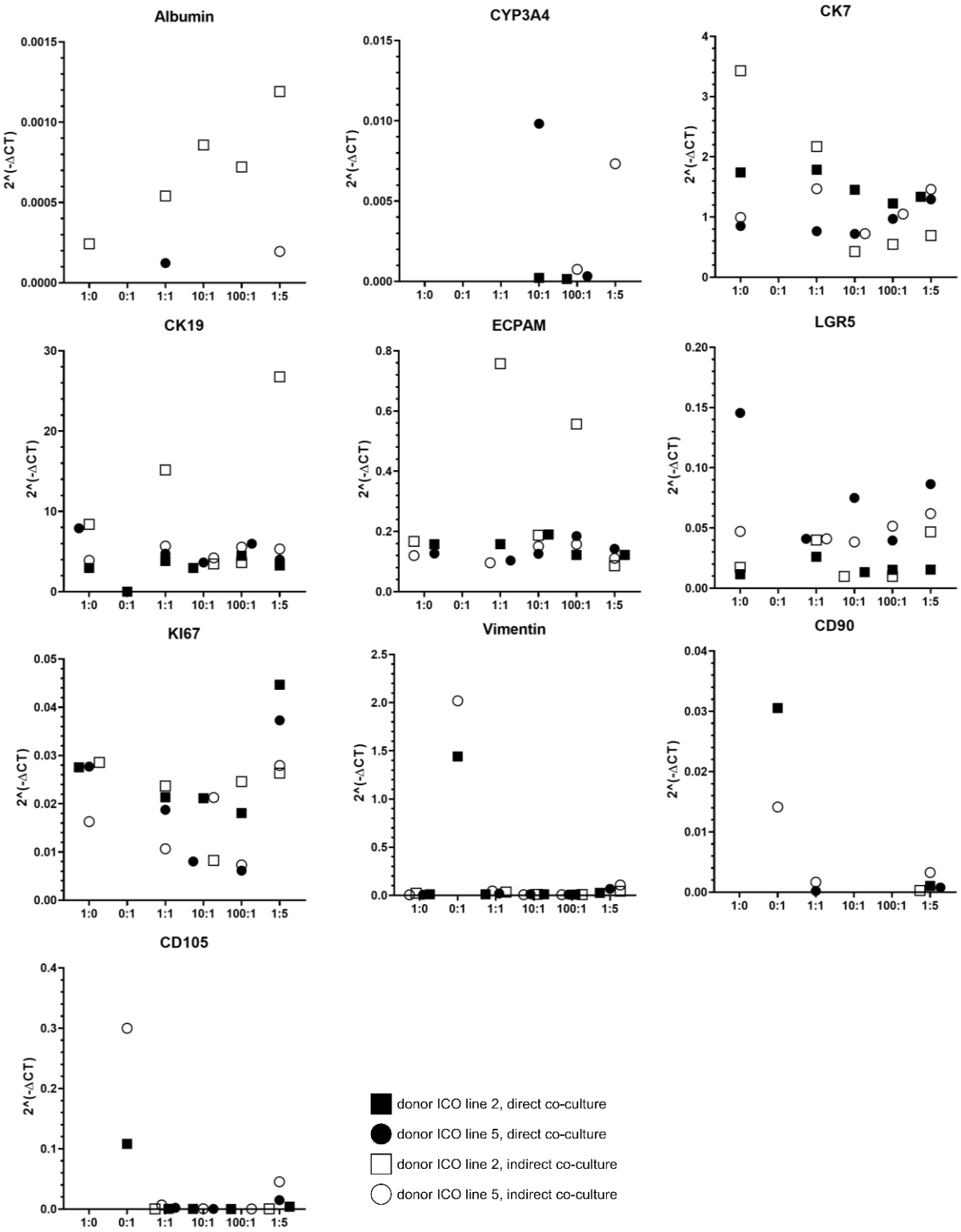

Figure 10. RNA expression data of the indirect versus direct co-culture in BME (ICO:L-MSC). Expression of hepatocyte (Albumin and CYP3A4), cholangiocyte (CK7, CK19, and EPCAM), stem cell (Lgr5), proliferation (KI-67), and MSC (Vimentin, CD90, and CD105) markers are shown if detectable. Data is displayed as $2^{-\Delta Ct}$. No major differences in gene expression were observed between the direct and indirect co-culture samples. Albumin and CYP3A4 expression were low or undetectable. The mean expression of MSC markers CD90, CD105, and Vimentin are highest in the L-MSC-only condition. Mean expression of CK7, CK19, Lgr5, KI-67, and EPCAM of indirect co-culture samples remained stable between conditions, except for 5 outliers in CK7, CK19, and EPCAM expression.

3.2 Cultures on ECM

After the co-cultures in BME, ICOs and L-MSCs were cultured on adult liver-derived ECM scaffolds to recreate the liver microenvironment more closely and to test the recellularization potential of the cells. Successful recellularization of these cells is an important step towards creating bioengineered liver tissue in the future.

3.2.1 Culture of ICOs and L-MSCs separately

3.2.1.1 Recellularization of ECM by ICOs

Mono-cultures give insight into normal growth patterns and recellularization capacity of ICOs on liver-derived ECM. Therefore, around 25,000 ICO cells were seeded onto a scaffold and cultured for three weeks. On the first day after seeding, single cells were observed. On days 4-7 of culture, the cells formed colonies and blasts that were located on top of the ECM and the plastic (see Figure 11A). After 10-14 days, the blasts had shrunken, and a monolayer of organoid cells became visible on top of the ECM and the plastic. In days 14-21, the blast mostly disappeared, and the organoid monolayer became the dominant growth pattern. This monolayer can be hard to detect with a brightfield microscope but is recognizable by the semi-transparent rim located at the borders of the ECM and by the polygonal cell pattern on top of the ECM (see Figure 11B and C). H&E staining showed that the cells did not penetrate the scaffold, but only grew on top of the ECM (see Figure 11D). F-actin staining in whole-mount confocal images revealed the polygonal shape and honeycomb-like structures of the monolayer of cells (see Figure 11E).

3.2.1.2 Morphology and viability of L-MSCs cultured on liver-derived ECM

As L-MSCs are normally expanded on a plastic surface in 2D, the recellularization capacity had to be tested before designing the direct co-culture models on ECM. Therefore, L-MSCs were cultured on liver-derived ECM scaffolds in EM. After one week of culture, L-MSCs were spread out on top of the ECM as can be seen in Figure 12B. Calcein staining (see Figure 12A and B) showed that cells remained viable after three weeks of culture. Compared to L-MSC culture in BME, the cells appeared to be slightly thicker and they maintained their fibroblast-like morphology for the culture period of three weeks. Similar to ICOs, L-MSCs grew on top of the ECM and did not seem to penetrate the ECM (see Figure 12C).

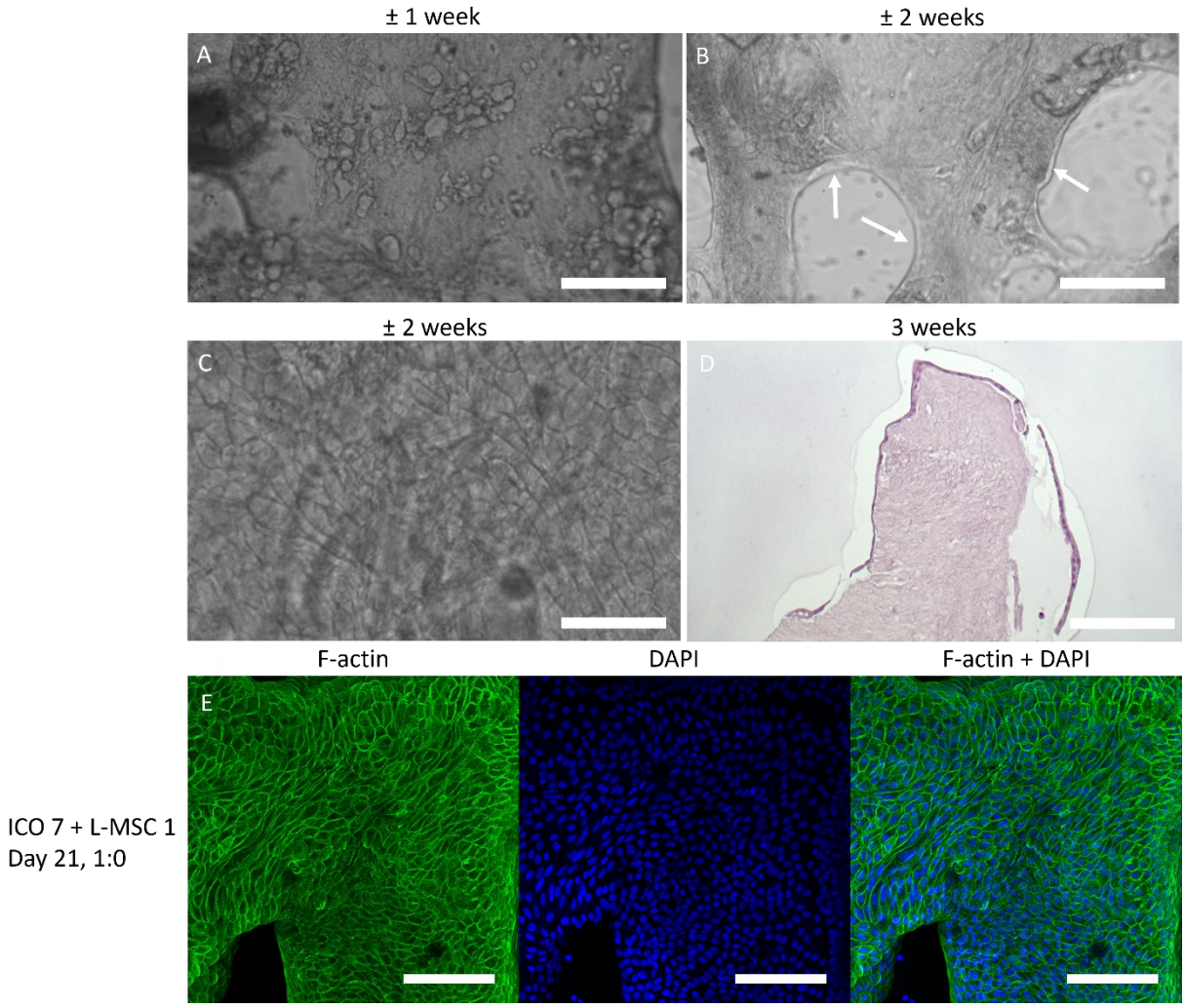

Figure 11. Brightfield images (A, B, C) and H&E staining (D) of ICO culture on ECM. Scale bars represent 200 µm (A, B, E), 100 µm (C, E), and 500 µm (D). Blast forming of organoid cells was visible after a week of culture (A). After two weeks of culture, a monolayer of organoid cells covered the ECM surface, visible by the transparent rim (B) and polygonal cell pattern (C). H&E staining of sections showed that organoid cells grew on top of the ECM, not penetrating the ECM (D). F-actin staining of whole scaffolds showed the polygonal shapes and honeycomb-like structures of the organoid cells (E).

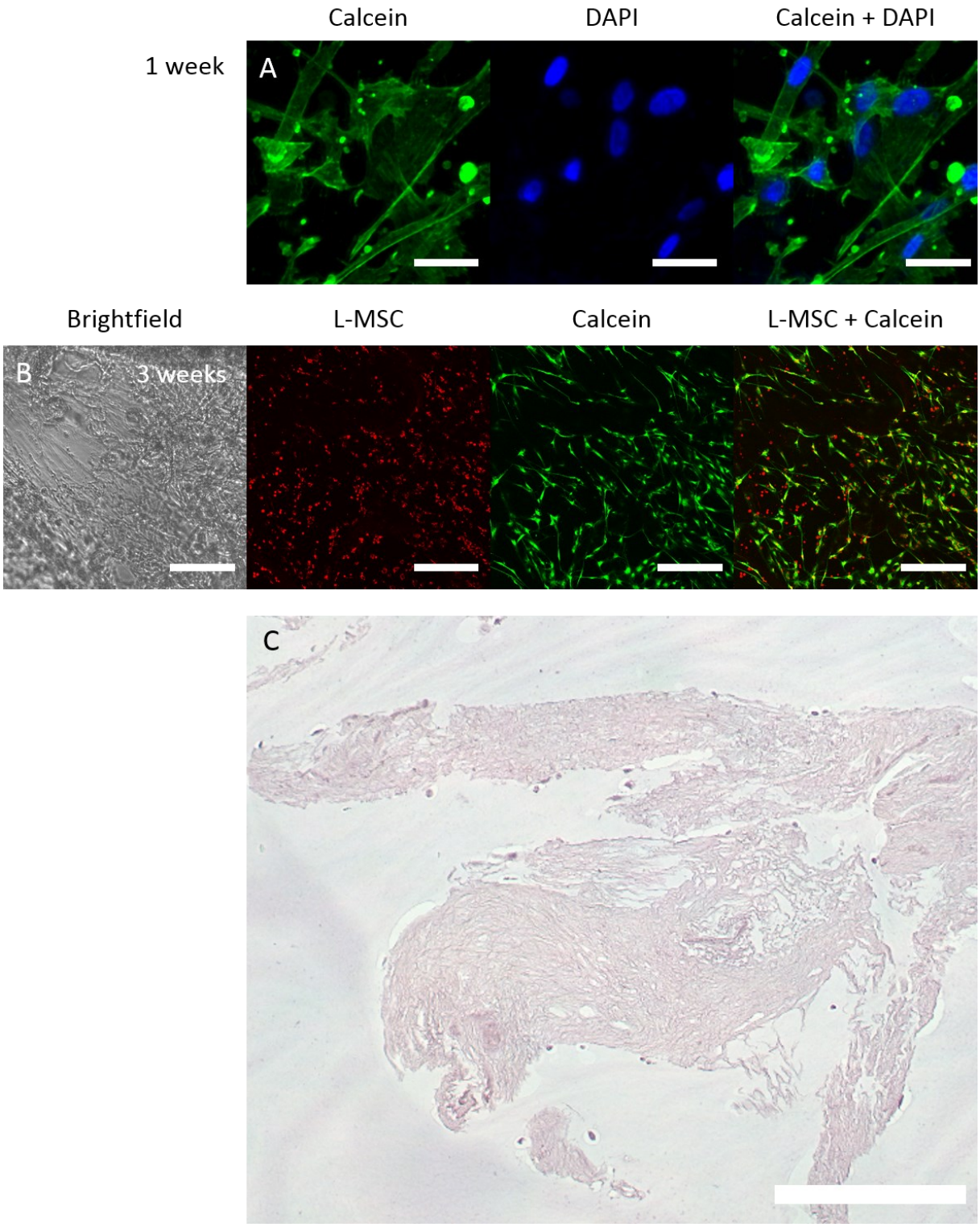

Figure 12. Calcein staining of the scaffolds after one (A) and three (B) weeks of culture and H&E staining of a section after 3 weeks of culture (C). Scale bars represent 100 (A), 400 (B, C) µm. Calcein staining showed that cells remained viable and revealed the fibroblast-like morphology of the cells (A, B). Nuclei were made visible using DAPI and L-MSCs were stained with the red cell dye. H&E staining revealed that cells only grew on top of ECM, not penetrating the scaffold (C).

3.2.2 Direct and MSC-first direct co-culture

ICOs and L-MSCs were cultured together in different ratios on liver-derived ECM scaffolds, allowing the cells to have cell-ECM interaction in addition to cell-cell interaction. In the direct co-culture model, where both cell types were added to the ECM simultaneously, ICO cells overtook the ECM surface, making it hard to detect L-MSCs in later stages of culture. Therefore, a second variant was tested: the MSC-first co-culture model. In this model, L-MSCs were seeded three days prior to the ICO cells, in the assumption that the L-MSCs would be more resilient and better detectable after three weeks of culture. In this section, the main results will be discussed. An overview of brightfield images of all culture conditions can be found in Appendix F.

3.2.2.1 Effect of L-MSCs on morphology and growth pattern of ICOs

In general, no large differences in ICO growth patterns were observed between the ICO-only and co-culture conditions. However, there was a clear difference in the amount of blast forming after 7-10 days of culture between the 1:1 and other conditions. The cultures of all donor ICO lines contained noticeably more blast-like structures than the ICO-only condition (1:0), as can be seen in Figure 13 and Appendix H. For two out of four donor ICO lines, increased blast forming was also observed in the 10:1 condition. Remarkably, the MSC-first 1:1 conditions did not contain an increased number of blasts compared to the ICO-only condition.

Between the direct and MSC-first direct co-culture samples, a difference in recellularization degree of the scaffolds was observed. In the direct co-culture samples, scaffolds were completely recellularized by confluent monolayers of ICO cells. The MSC-first direct co-cultures, on the other hand, contained small areas that were not covered by ICO cells. In these areas, L-MSCs were detected. Aside from the earlier seeding of L-MSCs in the MSC-first direct co-culture, the difference in recellularization degree might be explained by the shorter ICO culture time of 3 days.

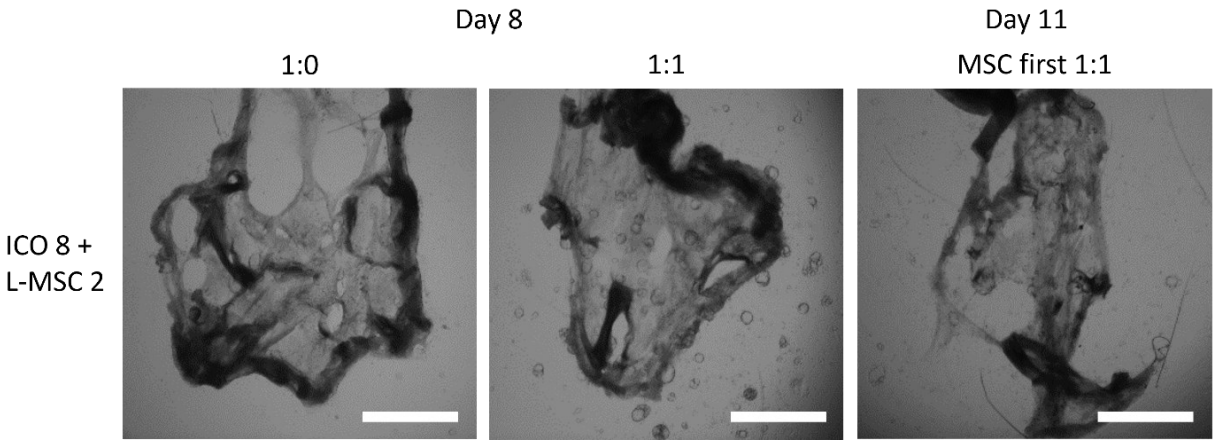

Figure 13. Brightfield images of scaffolds after a week of co-culture. Scale bars represent 1000 µm. The number of blast-like structures in the 1:1 condition was noticeably higher than in the control and MSC-first 1:1 conditions. For the MSC-first condition, day 11 is included to keep total ICO culture time constant, as the ICO cells have been seeded at day 4 and not day 1 for this condition. Images of other donor ICO lines can be found in Appendix H.

3.2.2.2 *Interaction of ICO cells and L-MSCs*

Direct cell-cell interactions in cultures on ECM were visibly distinct from those in BME cultures. In the early stages of culture, a mixture of L-MSCs and ICO cells was spread on the scaffold surface. Once the ICO cells began to form monolayers, L-MSCs started to disappear from these areas and clusters of L-MSCs were observed at the borders of the ICO monolayer. This is illustrated by the representable examples in Figure 14. Especially in the last week of culture, clumps of L-MSCs had detached from the scaffold surface and were floating in the medium. Based on these observations, ICO cells seem to be more dominant, pushing away L-MSCs during colonization of the ECM and the plastic surface around the scaffold.

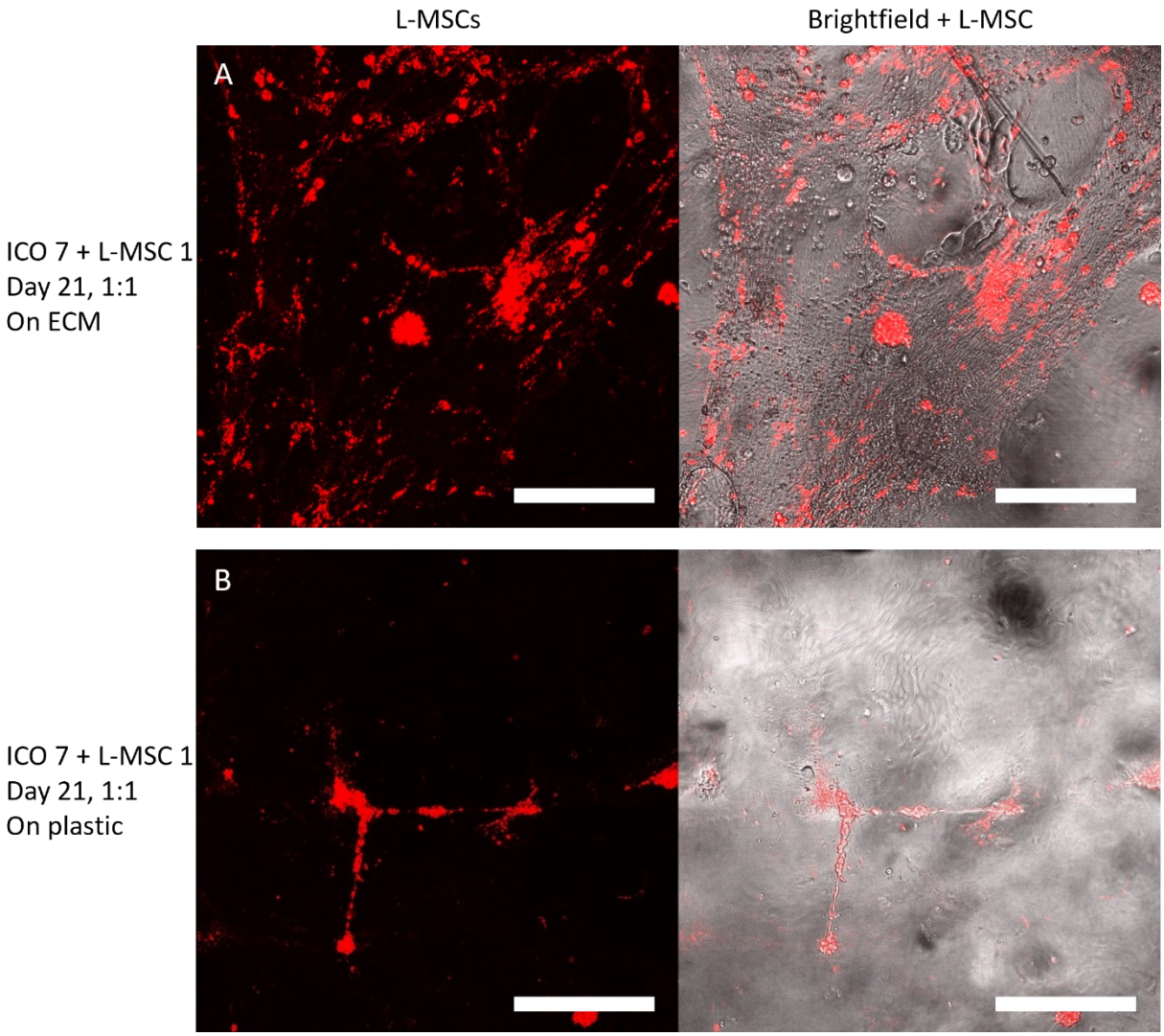

Figure 14. Confocal images of the 1:1 condition of the direct co-culture on ECM at day 12. Scale bars represent 200 µm. L-MSCs are red fluorescent. Monolayers of ICO cells appear smoother than the ECM in images and have a wave-like pattern. In A, the organoid monolayers are visible at the left border, in the right bottom corner, and in the oval shapes in the right upper part of the image. Large clusters of L-MSCs (red) were visible at the edges or floating on top of ICO monolayers. In B, the entire surface is covered by an ICO monolayer. Only small numbers of L-MSCs were present in between the ICO cells of monolayers. The large L-shaped red signal comes from multiple L-MSCs that have clustered together.

3.2.2.3 CK19 expression

To assess CK19 expression, immunohistochemical analysis was performed on sections of the co-cultures on ECM. The presence of the L-MSCs did not affect the CK19 expression of ICO cells. In all conditions of the direct and MSC-first direct co-cultures, ICO cells were CK19 positive. Figure 15A and B show representable examples of sections of the 1:0 and 1:1 conditions of the direct co-culture. In addition, CK19 staining shows the polygonal shape of the ICO cells, with a lack of signal in the cell nuclei.

Literature shows contradictory results regarding CK19 expression of L-MSCs [37]. Unfortunately, it was hard to detect cells in sections of the L-MSC-only condition. The few cells that were detected, were CK19 negative (see Figure 15C). In the co-culture conditions, it was also hard to detect (potential) L-MSCs. In some of the sections, it was possible to identify nuclei of cells that were CK19 negative and were not part of the organoid monolayer (see Figure 15D).

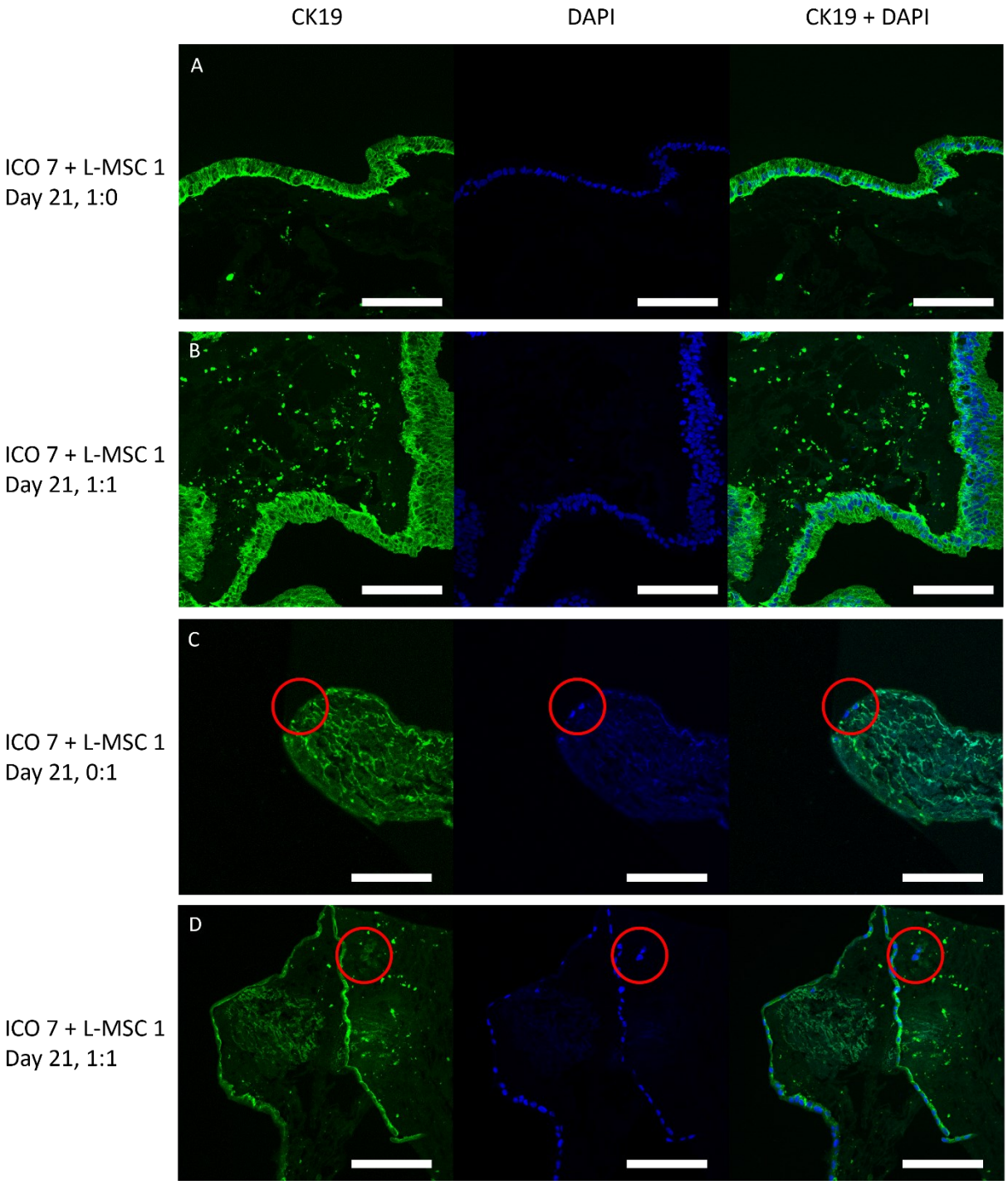

Figure 15. Confocal images of sections of the 1:0, 0:1, and 1:1 direct co-culture on ECM. Scale bars represent 100 µm. Sections were stained for the cholangiocyte marker CK19 and nuclei were made visible using DAPI. ICO cells were CK19 positive and grew in polygonal-shaped cell layers. CK19 negative cells, indicated by the red circles, are potential L-MSCs.

3.2.2.4 CK7 expression

To assess CK7 expression, immunohistochemical analysis was performed on whole scaffolds of the direct and MSC-first direct co-culture. During imaging, the scaffolds did not lie flat and folding was observed. This folding impacts the way the shape and number of cells are perceived in confocal images, especially when calculating nuclei count or areas. By focussing on the flatter parts of images, the impact of folding on these calculations was kept as limited as possible. Between the direct and MSC-first direct co-culture samples, a difference in ICO recellularization degree was observed after three weeks of culture, as described before. In short, in the direct co-culture, the ICO cells were able to completely recellularize the ECM and no L-MSCs were observed. In the MSC-first direct co-culture model, samples contained small areas that were not covered by ICO cells, and patches of L-MSCs were visible. As a result, the CK7 expression of only ICO cells was analyzed in confocal images of the direct co-culture samples. In the MSC-first direct co-culture samples, CK7 expression of both cell types was assessed.

All direct co-culture samples showed large numbers of CK7 positive cells (see Figure 16A-E). Confocal images of the 100:1 condition were notably different, as can be seen in Figure 16D. More stretched cells were visible, cells were larger, and less CK7 signal was visible than the other conditions. Calculating the CK7 positive area in images of samples (N=1) showed that the CK7 expression in the 100:1 condition was 16-21% lower than in the other conditions (see Figure 16E). Calculations on the same images revealed that the nuclei density varied between conditions (see Figure 16F). The lowest nuclei density was observed in the 100:1 condition, which is in line with the previous observation that cells appeared larger than in other conditions. Variance within one sample was observed, and therefore there will most likely be variance across samples of the same condition as well. Because only one sample per condition was imaged, the divergent results for the 100:1 condition could be an outlier. Additionally, a difference in scaffold alignment between samples could explain the divergent result of the 100:1 condition.

In MSC-first direct co-culture samples, both confluent layers of ICO cells and patches of the larger, fibroblast-like L-MSCs were observed (Figure 17). In the 1:1 condition sample, monolayers of ICO cells alternated with clusters of L-MSCs (see Figure 17A and B). In the 10:1 condition sample, ICO cells with cyst-like structures instead of honeycomb-like structures were found. Within one of these structures, CK7 negative cells were detected that could be L-MSCs (see Figure 17C). The red signal from L-MSCs was speckled and mostly located around the cell nuclei. However, signal of CK7 positive cells is expected to come from the whole plasma membrane, not only from the nuclei or the area around it. Therefore, the L-MSC signal is probably caused by leftover red cell dye, and the cells are most likely CK7 negative, especially in comparison to the CK7 positive ICO cells.

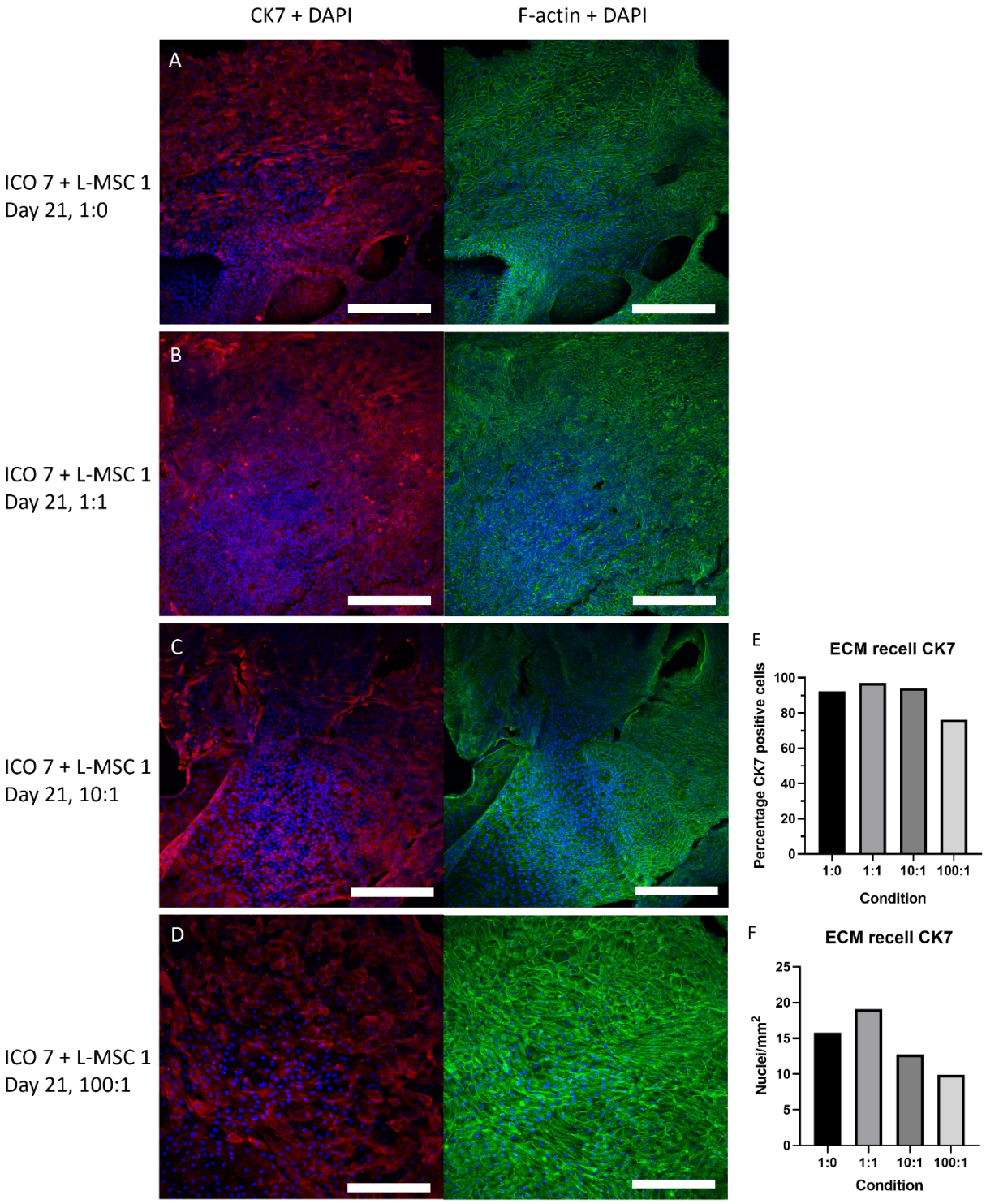

Figure 16. Whole-mount imaging of the direct co-culture samples. Scale bars represent 200 µm (A-D). Samples contained confluent monolayers of CK7 positive organoid cells (A-D). The 100:1 condition (D) showed slightly lower numbers of CK7 positive cells. Calculation of the percentage of CK7 positive area in images (E) showed difference in CK7 positivity of around 16-21% between the 100:1 and other conditions (1:0 ~ 92%, 1:1 ~ 97%, 10:1 ~ 94%, 100:1 ~ 76%). Nuclei count (F) varied between different conditions. (1:0 ~ 16, 1:1 ~ 19, 10:1 ~ 13, 100:1 ~ 10).

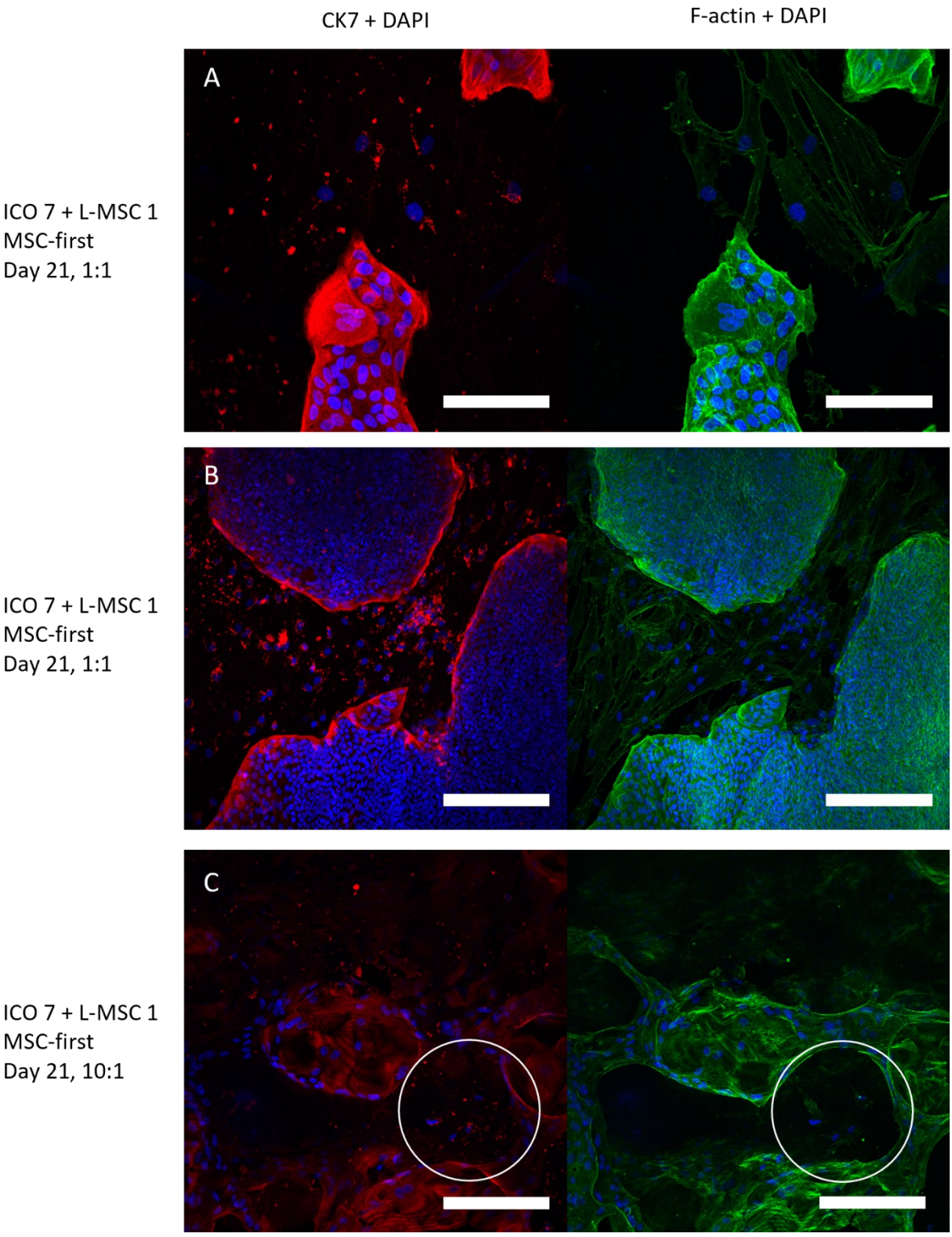

Figure 17. Whole-mount imaging of the MSC-first direct co-culture samples. Scale bars represent 100 (A) and 200 (B, C) µm. Both monolayers of ICO cells and L-MSCs were present. The ICO cells were smaller than L-MSCs and CK7 positive. L-MSCs had a fibroblast-like morphology and were most probably CK7 negative. The flecked red signal around the cell nuclei of L-MSCs is likely caused by leftover cell dye. In the circles (C), potential L-MSCs are visible. The two cell types did not seem to mix but were growing close to one another.

3.2.2.5 Gene expression of co-culture models on ECM

Gene expression was measured of all direct and MSC-first direct co-cultures (N=4), including a 1:0 and 1:1 (ICO:L-MSC) BME control condition. The data is summarized in Figure 18. Unfortunately, RNA extraction of the 0:1 conditions resulted in low concentrations (≤ 10 ng/µL) with questionable purity. Results are included but should not be used to draw definite conclusions. Matching multiple comparison tests showed statistically significant differences between the mean Vimentin and Lgr5 expression. However, post hoc tests were not able to detect statistically significant differences between two conditions.

In the majority of the samples, expression of the hepatocyte marker CYP3A4 was not detectable. Albumin expression was better detectable, though the expression was generally low. The highest Albumin expression was found in ECM samples containing ICOs and L-MSCs, with higher L-MSCs concentrations resulting in higher Albumin expression (on average 3.1-fold and 2.4-fold higher in the direct 1:1 and MSC-first direct 1:1 conditions compared to the ECM ICO-only condition). The mean expression of MSC markers CD90, CD105, and Vimentin, proliferation marker KI-67, and stem cell marker Lgr5 followed similar trends. Expression of these markers was highest conditions with high L-MSC concentrations. Remarkably, the mean expression of the MSC-first direct 1:1 condition was higher than the direct 1:1 condition (CD90: 3.9-fold, CD105: 3.3-fold, Vimentin: 2.3-fold, KI-67: 1.3-fold and Lgr5: 2.0-fold higher). Additionally, the mean Lgr5 and KI-67 expression in the BME 1:1 condition was notably higher than in the direct 1:1 and MSC-first direct 1:1 conditions (on average 2.9-fold and 4.3-fold higher than the direct 1:1 condition). The mean expression of the cholangiocyte markers was both up- and downregulated in co-culture conditions compared to the ECM ICO-only condition. Mean EPCAM and CK19 expression were slightly higher in direct and MSC-first direct co-culture conditions (on average 1.4-fold, SD:±0.24 and 1.5-fold, SD:±0.5). On the other hand, mean CK7 expression was lower in co-culture conditions (on average 1.3-fold, SD:±0.1), except for the MSC-first direct 10:1 condition. Contrary to the immunohistochemistry results, expression of CK7 and CK19 was observed in the L-MSC-only condition (0:1). Moreover, the mean CK7 expression of the direct 100:1 condition was slightly higher than the direct 1:1 and 10:1 conditions.

In conclusion, the expression of hepatocyte markers was low for all conditions. L-MSCs did not have a clear effect on the expression of cholangiocyte markers, since both up- and downregulation was observed. On the contrary, L-MSCs did have a clear effect on the expression of MSC markers CD90, CD105, and Vimentin, proliferation marker KI-67, and stem cell marker Lgr5. Mean expression was highest in conditions with high L-MSC concentrations and went down as the L-MSC concentration went down.

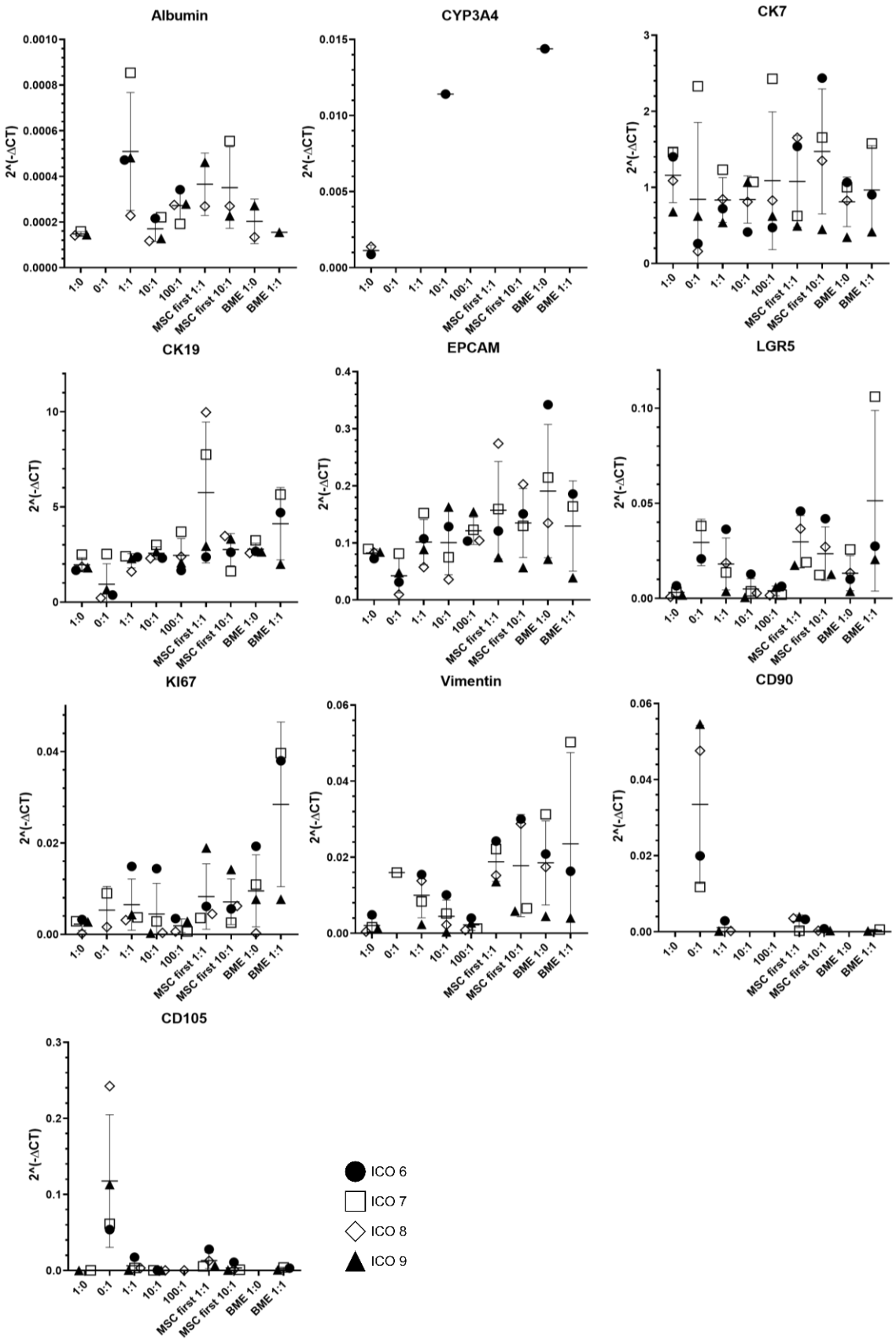

Figure 18. RNA expression data of direct, MSC-first direct co-culture on ECM and control conditions in BME (ICO:L-MSC). Expression of hepatocyte (Albumin and CYP3A4), cholangiocyte (CK7, CK19, and EPCAM), stem cell (Lgr5), proliferation (KI-67), and MSC (Vimentin, CD90, and CD105) markers are shown if detectable. Data is displayed as $2^{-\Delta Ct}$. Expression of hepatocyte markers was low or undetectable. Expression of MSC markers CD90, CD105, and Vimentin, proliferation marker KI-67, and stem cell marker Lgr5 was highest in conditions with high L-MSC concentrations and went down as the L-MSC concentration went down. L-MSCs did not have a clear effect on the expression of cholangiocyte markers, as both up- and downregulation was observed.

4 Discussion

Although existing *in vitro* liver models give insight into liver function and development, they are still too simplistic and unable to model the full liver function. Therefore, improvement of *in vitro* models is essential to enhance the understanding of healthy and pathological liver function and to develop new treatments for end-stage liver disease. In this study, adult human liver-derived ICOs, L-MSCs, and decellularized ECM were combined in co-culture models as a step towards complex liver models that include the relevant components of the native tissue.

4.1 Cultivation of ICOs in the presence of L-MSC derived CM

MSC-derived CM can be a rich source of biomolecules like soluble proteins, lipids, extracellular vesicles, and other compounds that aid in tissue repair and regeneration [32–34]. For this reason, the first step of this study was to assess the effect of the L-MSC secretome on ICOs by culturing ICOs in different types and concentrations of L-MSC-derived CM. These experiments showed that the presence of CM had no clear effect on ICO growth patterns and expression of hepatocyte, cholangiocyte, MSC, and proliferation markers. This result was unexpected, as similar experiments performed by Cordero-Espinoza *et al.* showed that CM of both freshly isolated and *in vitro* expanded $SCA1^+$ periportal MSCs enhanced organoid formation and proliferation of mouse-derived $EPCAM^+$ ductal cells significantly. In the second variant of the CM co-culture setup of this study, ICOs were differentiated towards hepatocytes. In these cultures, the expression of hepatocyte markers Albumin and CYP3A4 was downregulated in the presence of CM. This result was also unexpected, as previous research has shown increased function and viability of primary hepatocytes when co-cultured with MSCs [22,38].

The different effects of MSC-derived CM could be explained by a difference in (basal) culture medium composition. The study of Cordero-Espinoza *et al.* compared organoids cultured in basal medium (Adv. DMEM/F12 supplemented with Hepes, Penicillin/Streptomycin, Glutamax, 1% B27, 1% N2 and 1.25mM N-acetylcysteine) to organoids cultured in a mixture of this basal medium and $SCA1^+$MSC-derived CM. For the CM co-cultures of this study, CM was mixed with a growth factor supplemented medium (EM). Therefore, the L-MSC-derived CM might have enhanced organoid formation and proliferation similarly as in the experiments of Cordero-Espinoza *et al.*, but since the EM is already optimized to promote organoid expansion, this effect could have been undetectable. In future experiments, L-MSC-derived CM could be mixed with a growth factor depleted medium to test the capacity of the CM to promote organoid formation and proliferation.

Another explanation for the different effects of CM is a difference in CM composition. The type and quantity of growth factors and cytokines secreted by MSCs depend on several factors, like culture conditions and the growth phase of the cells. These factors were most likely not constant between this study and the study of Cordero-Espinoza *et al,* resulting in different CM compositions and biological activity. In addition, the biomolecules released by MSCs in mono-culture can differ from those released in co-culture conditions. This can explain why L-MSC-derived CM downregulated the expression of hepatocyte markers, while other studies show increased hepatocyte function in co-culture models. Because the composition of the CM used in this study was not analyzed, it is a “black box”. However, other studies have shown that important biomolecules secreted by MSCs include VEGF, PEDF, TGF- β1, FGF-2, HGF, IGF-1, SCF, and IL-6 [39,40]. This suggests that there is an overlap between the growth factors that are present in L-MSC-derived CM and EM, which contributes to the assumption that L-MSCs could enhance organoid formation and proliferation. Future studies could identify the composition of the L-MSC-derived CM. This will aid in confirming this assumption and explaining the effects of CM that were observed in this study. Moreover, this analysis will make comparisons with other CM types easier, and can also be used to measure batch-to-batch variation between CM of one and different donor L-MSC lines. In addition, the functional activity of the CM could be tested with a variety of assays, like the scratch wound healing assay that measures the effect of CM on cell migration.

4.2 Co-cultivation of ICOs and L-MSCs in BME

Because of the limited effect the L-MSC-derived CM had on ICO growth and gene expression in this study, more complex indirect and direct BME co-culture models were created that allowed the cells to interact and create direct cell-cell contact. Cordero-Espinoza *et al.* created similar direct and indirect (transwell) co-culture models. They found that organoid formation and proliferation was stimulated by the presence of MSCs in indirect co-culture models, similarly as in the CM models. Remarkably, direct co-culture models showed divergent results depending on the organoid:MSC ratio. Ratios of 10:≤1 increased organoid formation, similar to CM and indirect culture. On the other hand, higher MSC ratios decreased the organoid formation efficiency. Combining these observations, they concluded that paracrine MSCs signals (indirect cell-cell contract) enhance organoid proliferation, and juxtacrine signals (direct cell-cell contact) decrease proliferation. In this study, however, only small differences in ICO formation and gene expression were observed between the direct and indirect co-culture models and different ICO:L-MSC ratios. Moreover, in both direct and indirect BME culture models, conditions with high ratios of L-MSCs (1:5 conditions) showed the highest mean expression of proliferation marker KI-67. Lower L-MSC concentrations (1:1, 10:1, and 100:1 conditions) resulted in downregulation of the proliferation marker compared to the ICO-only condition. However, little direct cell-cell contact was observed in these cultures, suggesting minimal juxtracrine signaling. This could explain why no decrease in organoid formation efficiency was observed in conditions with high L-MSCs concentrations in the culture models of this study.

Although this study and the study of Cordero-Espinoza *et al.* included liver-derived MSCs, the cells originate from different species and are not necessarily collected from the same site in the liver. Cordero-Espinoza *et al.* isolated mesenchymal cells specifically from periportal sites, ensuring that these MSCs are in close proximity to cholangiocytes *in vivo*. On the other hand, it is difficult to determine the original location of the L-MSCs derived from liver perfusate. Therefore, the L-MSCs are possibly not in close proximity with cholangiocytes *in vivo*. Unfortunately, it is hard to compare both MSC types since analyzed markers hardly overlap. Nevertheless, it is known that both MSC types lack the expression of CD45, and literature shows that perfusate-derived L-MSCs are CD34 negative, whereas the $SCA1^+$ MSCs do express CD34 [31]. This suggests that the MSC types are distinct from one another and might have different functionality. Because the MSCs used by Cordero-Espinoza *et al.* are located in the periportal site of the liver and express SCA1 and CD34 but lack the expression of CD45, it might be interesting to include oval markers A6 and α-fetoprotein in future analyses [41].

4.3 Co-cultivation of ICOs and L-MSCs on ECM

For the first co-culture models of this study, ICOs and L-MSCs were cultured in BME. However, BME is made up of compounds derived from mouse tumor tissue, limiting the clinical applications of BME based models [27]. ECM, on the other hand, has the protein composition, and 3-dimensional and physiological properties of the original tissue and can potentially be used for clinical applications. Therefore, the recellularization capacity of ICOs and L-MSCs was assessed by culturing both cell types on liver-derived ECM scaffolds.

The recellularization of ICOs on liver-derived scaffolds has already been established before. For example, Willemse *et al.* recellularized EBD with intra- and extrahepatic liver organoids (IDO and EDO) [42]. They found that EDO cells formed a confluent monolayer with a “honeycomb”-like structure on top of the scaffold and expressed CK7 and CK19. The observations in this study are in line with the observations of Willemse *et al.*, as the ICOs in the direct and MSC-first direct cultures showed similar growth patterns and were also CK7 and CK19 positive.

MSCs have been used to recellularize all different types of scaffolds, including heart, kidney, and lung-derived ECM. MSCs attached to the periphery of the scaffolds, and some studies also show infiltration of the ECM [43]. In this study, L-MSCs seemed to only grow on the periphery of the ECM. Cells were probably CK7 and CK19 negative on protein level, although it was difficult to determine

CK19 expression in stained sections. Wei-Cheng *et al*. recellularized liver ECM with MSCs, and found that cells started to express CK19 after 4 weeks of culture [44]. Additional experiments should be performed to determine if L-MSCs also start to express CK19 after multiple weeks of culture. The distribution and migration of the MSCs on scaffolds is influenced by factors like composition and stiffness of the ECM, medium composition, and static and dynamic culture. Therefore, cell distribution results can differ depending on the used culture conditions [45]. Additionally, Liver-derived ECM can influence the differentiation of MSCs and (induced) pluripotent stem cells towards cholangiocytes or hepatocytes [46,47]. For example, the studies of Jiang *et al.* and Li *et al.* have shown that liver-derived ECM improves MSC differentiation efficiency towards hepatocytes [44,48]. In this study, L-MSCs remained their elongated fibroblast-like morphology after three weeks of culture on scaffolds. In the L-MSC-only conditions, gene expression of hepatocyte markers Albumin and CYP3A4 was undetectable. In co-culture conditions, the expression was very low or undetectable. Overall, no indication of differentiation towards hepatocytes was observed. Gene expression of CK7, CK19, and EPCAM was detectable in ECM MSC-only conditions, whereas no detection was seen in the BME MSC-only conditions. This could indicate that MSCs differentiate towards cholangiocytes or hepatic progenitor cells in the presence of liver-derived ECM. However, RNA extraction of the MSC-only conditions resulted in low concentrations with questionable purity, and gene expression results can therefore not be used to draw definitive conclusions.

In both the direct and MSC-first direct co-culture conditions of this study, ICO cells were able to recellularize the scaffold. However, a difference in the recellularization degree of ICOs was observed. In MSC-first models, scaffolds were not completely covered by ICOs, indicating that these conditions were less ideal for recellularization of ICOs. In direct cultures, the presence of the L-MSCs had no clear effect on the recellularization capacity of ICOs. In mono-culture, L-MSCs were capable of recellularizing liver-derived ECM and remained viable for three weeks. However, in combination with ICOs, L-MSCs were not able to repopulate the scaffolds since they were pushed away. Although L-MSC did not successfully recellularize the ECM in co-culture conditions and no clear beneficial effects on the recellularization capacity of ICOs were observed, L-MSCs should not be disregarded in future tissue engineering experiments. The cells can potentially improve the success rates of bioengineered liver tissue as biliary constructs in clinical settings by improving cell function of secondary cell types (e.g., cholangiocytes and hepatocytes) or by releasing anti-inflammatory factors. Zhang *et al.* tested the safety and potential of using MSCs in combination with engineered bile stents in pigs [49]. The immersion of the tissue around the stent in an MSC suspension during the procedure showed promising results. MSCs engrafted the bile duct wall, prevented anastomotic fibrosis, and promoted neoangiogenesis.

Because the ICOs and L-MSC grew only on the periphery of the scaffolds, the cultures are more two-dimensional than three-dimensional. To create 3D models, liver-derived ECM hydrogels can be used. Research has shown that these hydrogels are promising biomaterials since tissue-specific ECM helps to maintain cell phenotype and promote proliferation [50]. Moreover, they can promote organoid formation and induce the formation of more complex three-dimensional biliary networks [51,52]. Similar to decellularized scaffolds, liver-derived ECM hydrogel models have the potential to be used for clinical applications.

4.4 General remarks on MSC activities

Overall, L-MSCs had no clear effect on growth patterns and gene expression of ICOs in the experiments performed in this study. Furthermore, very little visible cell-cell contact was observed in BME models, and cells did not mix well in ECM models. Aside from the aforementioned reasons, there are more possible explanations for the limited visible effect on ICO growth and gene expression. *In vivo*, MSCs seem to be primarily active in damaged tissue, where they help to repair this damage and regulate the immune response. In our models, the L-MSCs probably do not get signals similar to those found in damaged tissue. As a result, the cells might not be activated, hence the accompanying combination of biomolecules, e.g., growth factors and cytokines, are not released. This could explain why no clear effect of the L-MSCs on ICOs was observed in this study.

MSCs have a high differentiation potential, which is regulated by the transcription and growth factors in the environment. Factors like medium composition, culture surface, and *in vitro* aging can alter the phenotype and differentiation potential of the MSCs [53,54]. Therefore, it is possible that the MSC function varied amongst the different co-culture models of both this and comparable studies since the culture environment was not constant between the models. The presence of the ECM, for example, might enhance the hepatic commitment of L-MSCs, as liver-derived ECM has been shown to improve MSC differentiation efficiency towards hepatocytes [44]. The change of MSC to EM medium can also significantly alter the L-MSC phenotype. Because the focus of this study was on ICO growth, organoid-specific culture medium was used in the BME and ECM co-culture models. However, L-MSCs thrive best in medium that contains serum (MSC medium). Although the morphology of L-MSCs was similar in EM and MSC medium cultures, studies have shown that changing the culture medium composition can significantly affect the phenotype of cells. For example, Hagmann *et al.* discovered that different expansion media compositions had a significant impact on CD90 and CD105 expression of MSCs [55]. To assess whether the lack of visible effect of L-MSCs on ICOs is related to the choice of culture medium, different medium compositions could be tested in future studies. To enhance L-MSC functionality, EM can be supplemented with WNT CM (like in the study of Cordero-Espinoza *et al.*) and/or (low percentages of) serum. An alternative method is to supplement serum-free MSC media formulations such as the PPRF-msc6 medium with the desired medium components [56].

Overall, it would be beneficial to assess the phenotype and viability of L-MSCs in future studies. This will allow for the comparison of L-MSC function between different models and donor lines. Additionally, the effects of different culture environments on L-MSC phenotype and viability could be determined. This information is valuable for finding optimal culture conditions for future co-culture models. Gene expression profiling can contribute to the global picture of cellular function. Assessing the metabolic activity, differentiation capacity, and immunoregulatory features of cells will also provide useful information on cellular function.

4.5 General optimizations of future co-culture models

Several studies focused on mesenchymal-ductal cell interaction of various cell types like HSCs and portal (myo)fibroblasts. However, no studies were found that included perfusate-derived L-MSCs. Because there is no in-depth understanding of the interaction between L-MSCs and the ductal environment, the limited effect of L-MSCs on ICO culture could indicate that these cells have also little interaction *in vivo*. If this would be the case, optimizing the co-culture model will not result in an increased effect of L-MSC on ICOs. The focus can be shifted to other co-culture candidates to achieve more cell-cell contact. Cells such as hepatocytes, HSCs, Kupffer cells, and LSECs are all promising candidates because they perform key roles and make up the majority of the liver tissue. The co-culture models created in this study can be used as a base for future ICO co-cultures, as L-MSCs can be replaced by other cell types. However, finding culture conditions that allow both cell types to maintain their phenotype and viability will remain a big challenge. In addition, the co-culture models can be optimized to improve future models. Besides the aforementioned suggestions (e.g. assessing the composition of the CM, using growth factor depleted medium, and liver-derived ECM hydrogels), more optimizations can be thought of.

First, the RNA derived from ICO and L-MSC could be kept separate. In this study, the gene expression was measured using a mixture of ICOs and L-MSCs derived RNA. Therefore, it is not possible to determine the ICO and L-MSC related contribution. For a number of genes, expression was relatively high in conditions with high L-MSC ratios. Since these conditions presumably include relatively more L-MSC-derived RNA than conditions with low L-MSC concentrations, this effect could be attributed to L-MSC-related expression. However, this cannot be confirmed for the performed experiments. Therefore, it would be beneficial to split the cells in future experiments to prevent the RNA from mixing. This can be achieved by keeping the cells separated during culture by using indirect co-culture techniques like transwell systems, or cells can be sorted (with a FACS-sorter) before RNA isolation.

Tracking and identifying both cell types is essential in co-culture models. The lentiviral transduction to integrate a red fluorescence protein gene and the red fluorescent lipophilic membrane dye were both functional methods to track the L-MSCs. However, in future research, both cell types should be labeled to prevent confusion in case of low detectability of stainings. Cells could also be identified by using cell-specific markers.

Last, in addition to analyzing the morphology of cells, visible interaction between cell types, and the expression of hepatocyte, cholangiocyte, MSC, and proliferation markers, it would be interesting to include more cell function assays. Cholangiocytes dilute and alkalinize the bile that is produced by hepatocytes. To execute these activities, cholangiocytes use several channels, transporters, and exchangers. Assays like the forskolin-induced swelling assay to test the cAMP-activated CFTR channel activity are available to test the ion-channel activity, and thus cell function of the ICOs.

5 Conclusion

In this study, co-cultures including ICOs and L-MSCs were created as a stepping stone towards complex models that represent the (complete) liver microenvironment. In the co-culture models in this study, the presence of the L-MSCs had no clear effect on ICO growth and the expression of hepatocyte, cholangiocyte, MSC, and proliferation markers. Recellularization experiments showed that both cell types were capable of repopulating the ECM. However, L-MSCs had no clear beneficial effect on ICO repopulation and cell types did not mix well on the scaffolds. Previous studies (e.g., the study of Cordero-Espinoza *et al.*) have shown that MSCs have the potential to promote cell function and organoid formation in co-culture models. Including a wider range of markers and functional assays might help to clarify why no clear effects were observed in this study.

Although no clear effects of L-MSCs were observed, the co-culture models developed in this study provide a valuable base for future co-culture research. In future experiments, the L-MSCs could be replaced with other liver-derived cell types that potentially have a beneficial effect on ICO growth and viability. The models have to be adjusted to the “new” cell type to create the optimal co-culture environment, but similar setups can be used to analyze the effects of secreted factors, indirect and direct cell-cell contact, cell-ECM contact, and the recellularization potential of cells.

In the ultimate liver model, all relevant components of the microenvironment are included and functional bioengineered liver tissue is created. These models can be used for multiple applications, like disease modeling and drug screening. Moreover, bioengineered tissue has the potential to replace diseased tissue in patients. The recellularization setups of this study form a valuable basis since only human-derived cells and ECM were included. This opens the doors for personalized medicine approaches and autologous transplantation in the future. The setups can be expanded with additional components of the liver microenvironment as a step towards creating complex liver models. This can be done by adding additional liver-derived cell types, like combining hepatocytes, ICOs, and L-MSCs, in which L-MSCs could enhance hepatocyte function or differentiate towards hepatocyte-like cells. Another option is to culture the cells in organ-on-a-chip systems. In these systems, numerous parameters including dynamic flow, mechanical stimulation, and concentration gradients can be controlled.

Although there remain many challenges to overcome in order to create a “complete” liver model, this study has taken an important step by combining L-MSCs and ICOs in co-culture models. Especially the recellularization setups form a promising basis for the development of complex liver models since native tissue-derived ECM is included. Future studies should expand the setups with additional components of the liver microenvironment like adult liver-derived cells, and optimize culture conditions for all included cell types.

6 Bibliography

[1] M. Blachier, H. Leleu, M. Peck-Radosavljevic, D.C. Valla, F. Roudot-Thoraval, The burden of liver disease in Europe: A review of available epidemiological data, *Journal of Hepatology*. 58 593–608 (2013), doi:10.1016/j.jhep.2012.12.005.

[2] Z. Koledova, 3D cell culture: An introduction, in: Methods Mol. Biol., Humana Press Inc., 2017: pp. 1–11, doi:10.1007/978-1-4939-7021-6_1.

[3] H. Hu, H. Gehart, B. Artegiani, C. LÖpez-Iglesias, F. Dekkers, O. Basak, J. van Es, S.M. Chuva de Sousa Lopes, et al., Long-Term Expansion of Functional Mouse and Human Hepatocytes as 3D Organoids, *Cell*. 175 1591–1606 (2018), doi:10.1016/j.cell.2018.11.013.

[4] M. Huch, H. Gehart, R. Van Boxtel, K. Hamer, F. Blokzijl, M.M.A. Verstegen, E. Ellis, M. Van Wenum, et al., Long-term culture of genome-stable bipotent stem cells from adult human liver, *Cell*. 160 299–312 (2015), doi:10.1016/j.cell.2014.11.050.

[5] Y. Guan, D. Xu, P.M. Garfin, U. Ehmer, M. Hurwitz, G. Enns, S. Michie, M. Wu, et al., Human hepatic organoids for the analysis of human genetic diseases, *JCI Insight*. 2 (2017), doi:10.1172/jci.insight.94954.

[6] R. Ouchi, S. Togo, M. Kimura, T. Shinozawa, M. Koido, H. Koike, W. Thompson, R.A. Karns, et al., Modeling Steatohepatitis in Humans with Pluripotent Stem Cell-Derived Organoids, *Cell Metabolism*. 30 374-384.e6 (2019), doi:10.1016/j.cmet.2019.05.007.

[7] T. Takebe, K. Sekine, M. Enomura, H. Koike, M. Kimura, T. Ogaeri, R.R. Zhang, Y. Ueno, et al., Vascularized and functional human liver from an iPSC-derived organ bud transplant, *Nature*. 499 481–484 (2013), doi:10.1038/nature12271.

[8] J.M. Banales, R.C. Huebert, T. Karlsen, M. Strazzabosco, N.F. LaRusso, G.J. Gores, Cholangiocyte pathobiology, *Nature Reviews. Gastroenterology & Hepatology*. 16 269–281 (2019), doi:10.1038/S41575-019-0125-Y.

[9] Y. Nakanuma, Tutorial Review for Understanding of Cholangiopathy, *International Journal of Hepatology*. 2012 1–9 (2012), doi:10.1155/2012/547840.

[10] M.M.A. Verstegen, F.J.M. Roos, K. Burka, H. Gehart, M. Jager, M. de Wolf, M.J.C. Bijvelds, H.R. de Jonge, et al., Human extrahepatic and intrahepatic cholangiocyte organoids show region-specific differentiation potential and model cystic fibrosis-related bile duct disease, *Scientific Reports 2020 10:1*. 10 1–16 (2020), doi:10.1038/s41598-020-79082-8.

[11] P. Godoy, N.J. Hewitt, U. Albrecht, M.E. Andersen, N. Ansari, S. Bhattacharya, J.G. Bode, J. Bolleyn, et al., Recent advances in 2D and 3D in vitro systems using primary hepatocytes, alternative hepatocyte sources and non-parenchymal liver cells and their use in investigating mechanisms of hepatotoxicity, cell signaling and ADME, *Archives of Toxicology*. 87 1315–1530 (2013), doi:10.1007/s00204-013-1078-5.

[12] S.N. Bhatia, U.J. Balis, M.L. Yarmush, M. Toner, Effect of cell–cell interactions in preservation of cellular phenotype: cocultivation of hepatocytes and nonparenchymal cells, *The FASEB Journal*. 13 1883–1900 (1999), doi:10.1096/fasebj.13.14.1883.

[13] E.M. Horwitz, K. Le Blanc, M. Dominici, I. Mueller, I. Slaper-Cortenbach, F.C. Marini, R.J. Deans, D.S. Krause, et al., Clarification of the nomenclature for MSC: The International Society for Cellular Therapy position statement, *Cytotherapy*. 7 393–395 (2005), doi:10.1080/14653240500319234.

[14] M. Dominici, K. Le Blanc, I. Mueller, I. Slaper-Cortenbach, F.C. Marini, D.S. Krause, R.J. Deans, A. Keating, et al., Minimal criteria for defining multipotent mesenchymal stromal cells. The International Society for Cellular Therapy position statement, *Cytotherapy*. 8 315–317 (2006), doi:10.1080/14653240600855905.

[15] A.I. Caplan, D. Correa, The MSC: An injury drugstore, *Cell Stem Cell*. 9 11–15 (2011), doi:10.1016/j.stem.2011.06.008.

[16] A.I. Caplan, Mesenchymal stem cells: Time to change the name!, *Stem Cells Translational Medicine*.

6 1445–1451 (2017), doi:10.1002/sctm.17-0051.

[17] C.W. Lee, Y.F. Chen, H.H. Wu, O.K. Lee, Historical Perspectives and Advances in Mesenchymal Stem Cell Research for the Treatment of Liver Diseases, *Gastroenterology*. 154 46–56 (2018), doi:10.1053/j.gastro.2017.09.049.

[18] L. Dong, Y. Pu, X. Chen, X. Qi, L. Zhang, L. Xu, W. Li, Y. Ma, et al., HUCMSC-extracellular vesicles downregulated hepatic stellate cell activation and reduced liver injury in S. japonicum-infected mice, *Stem Cell Research and Therapy*. 11 1–11 (2020), doi:10.1186/s13287-019-1539-8.

[19] G. Chiabotto, C. Pasquino, G. Camussi, S. Bruno, Molecular Pathways Modulated by Mesenchymal Stromal Cells and Their Extracellular Vesicles in Experimental Models of Liver Fibrosis, *Frontiers in Cell and Developmental Biology*. 8 (2020), doi:10.3389/fcell.2020.594794.

[20] M. Alfaifi, Y.W. Eom, P.N. Newsome, S.K. Baik, Mesenchymal stromal cell therapy for liver diseases, *Journal of Hepatology*. 68 1272–1285 (2018), doi:10.1016/j.jhep.2018.01.030.

[21] Y. You, D.G. Wen, J.P. Gong, Z.J. Liu, Research Status of Mesenchymal Stem Cells in Liver Transplantation, *Cell Transplantation*. 28 1490–1506 (2019), doi:10.1177/0963689719874786.

[22] E. Fitzpatrick, Y. Wu, P. Dhadda, R.D. Hughes, R.R. Mitry, H. Qin, S.C. Lehec, N.D. Heaton, et al., Coculture With Mesenchymal Stem Cells Results in Improved Viability and Function of Human Hepatocytes, *Cell Transplantation*. 24 73–83 (2015), doi:10.3727/096368913X674080.

[23] L. Cordero-Espinoza, T.N. Kohler, A.M. Dowbaj, B. Strauss, O. Sarlidou, C. Pacini, R. Dobie, J.R. Wilson-Kanamori, et al., The proportion of periportal mesenchyme to ductal epithelial cells acts as a proliferative rheostat in liver regeneration, *BioRxiv*. (2020), doi:10.1101/2020.09.21.306258.

[24] S.D. Ramachandran, K. Schirmer, B. Münst, S. Heinz, S. Ghafoory, S. Wölfl, K. Simon-Keller, A. Marx, et al., In vitro generation of functional liver organoid-like structures using adult human cells, *PLOS ONE*. 10 (2015), doi:10.1371/journal.pone.0139345.

[25] A. Baiocchini, C. Montaldo, A. Conigliaro, A. Grimaldi, V. Correani, F. Mura, F. Ciccosanti, N. Rotiroti, et al., Extracellular matrix molecular remodeling in human liver fibrosis evolution, *PLOS ONE*. 11 (2016), doi:10.1371/journal.pone.0151736.

[26] R.G. Wells, Cellular Sources of Extracellular Matrix in Hepatic Fibrosis, *Clinics in Liver Disease*. 12 759–768 (2008), doi:10.1016/j.cld.2008.07.008.

[27] C. Hughes, L. Postovit, G. Lajoie, Matrigel: a complex protein mixture required for optimal growth of cell culture, *Proteomics*. 10 1886–1890 (2010), doi:10.1002/PMIC.200900758.

[28] G. Benton, I. Arnaoutova, J. George, H.K. Kleinman, J. Koblinski, Matrigel: from discovery and ECM mimicry to assays and models for cancer research, *Advanced Drug Delivery Reviews*. 79–80 3–18 (2014), doi:10.1016/J.ADDR.2014.06.005.

[29] T.J. Rowland, L.M. Miller, A.J. Blaschke, E.L. Doss, A.J. Bonham, S.T. Hikita, L.V. Johnson, D.O. Clegg, Roles of integrins in human induced pluripotent stem cell growth on Matrigel and vitronectin, *Stem Cells and Development*. 19 1231–1240 (2010), doi:10.1089/SCD.2009.0328.

[30] J. Willemse, M.M.A. Verstegen, A. Vermeulen, I.J. Schurink, H.P. Roest, L.J.W. van der Laan, J. de Jonge, Fast, robust and effective decellularization of whole human livers using mild detergents and pressure controlled perfusion, *Materials Science and Engineering C*. 108 (2020), doi:10.1016/j.msec.2019.110200.

[31] Q. Pan, S.M.G. Fouraschen, F.S.F.A. Kaya, M.M. Verstegen, M. Pescatori, A.P. Stubbs, W. van IJcken, A. van der Sloot, et al., Mobilization of hepatic mesenchymal stem cells from human liver grafts, *Liver Transplantation*. 17 596–609 (2011), doi:10.1002/lt.22260.

[32] C. Hu, L. Zhao, L. Zhang, Q. Bao, L. Li, Mesenchymal stem cell-based cell-free strategies: Safe and effective treatments for liver injury, *Stem Cell Research and Therapy*. 11 1–12 (2020), doi:10.1186/s13287-020-01895-1.

[33] B. Parekkadan, D. Van Poll, K. Suganuma, E.A. Carter, F. Berthiaume, A.W. Tilles, M.L. Yarmush, Mesenchymal stem cell-derived molecules reverse fulminant hepatic failure, *PLOS ONE*. 2 941 (2007), doi:10.1371/journal.pone.0000941.

[34] Z. Jiao, Y. Ma, Q. Zhang, Y. Wang, T. Liu, X. Liu, C. Piao, B. Liu, et al., The adipose-derived

mesenchymal stem cell secretome promotes hepatic regeneration in miniature pigs after liver ischaemia-reperfusion combined with partial resection, *Stem Cell Research and Therapy*. 12 1–12 (2021), doi:10.1186/s13287-021-02284-y.

[35] S. Akbari, G.G. Sevinç, N. Ersoy, O. Basak, K. Kaplan, K. Sevinç, E. Ozel, B. Sengun, et al., Robust, Long-Term Culture of Endoderm-Derived Hepatic Organoids for Disease Modeling, *Stem Cell Reports*. 13 627–641 (2019), doi:10.1016/j.stemcr.2019.08.007.

[36] M. Najimi, D.N. Khuu, P.A. Lysy, N. Jazouli, J. Abarca, C. Sempoux, E.M. Sokal, Adult-Derived Human Liver Mesenchymal-Like Cells as a Potential Progenitor Reservoir of Hepatocytes?, *Cell Transplantation*. 16 717–728 (2007). www.cognizantcommunication.com (accessed November 13, 2020).

[37] I. V. Kholodenko, L.K. Kurbatov, R. V. Kholodenko, G. V. Manukyan, K.N. Yarygin, Mesenchymal Stem Cells in the Adult Human Liver: Hype or Hope?, *Cells*. 8 1127 (2019), doi:10.3390/cells8101127.

[38] S.P. Rebelo, R. Costa, M.M. Silva, P. Marcelino, C. Brito, P.M. Alves, Three-dimensional co-culture of human hepatocytes and mesenchymal stem cells: improved functionality in long-term bioreactor cultures, *Journal of Tissue Engineering and Regenerative Medicine*. 11 2034–2045 (2017), doi:10.1002/TERM.2099.

[39] G. Sagaradze, O. Grigorieva, P. Nimiritsky, N. Basalova, N. Kalinina, Z. Akopyan, A. Efimenko, Conditioned Medium from Human Mesenchymal Stromal Cells: Towards the Clinical Translation, *International Journal of Molecular Sciences*. 20 (2019), doi:10.3390/IJMS20071656.

[40] A. Joseph, I. Baiju, I.A. Bhat, S. Pandey, M. Bharti, M. Verma, A. Pratap Singh, M.M. Ansari, et al., Mesenchymal stem cell-conditioned media: A novel alternative of stem cell therapy for quality wound healing, *Journal of Cellular Physiology*. 235 5555–5569 (2020), doi:10.1002/JCP.29486.

[41] C. Dorrell, L. Erker, K.M. Lanxon-Cookson, S.L. Abraham, T. Victoroff, S. Ro, P.S. Canaday, P.R. Streeter, et al., Surface markers for the murine oval cell response, *Hepatology*. 48 1282–1291 (2008), doi:10.1002/hep.22468.

[42] J. Willemse, F.J.M. Roos, I.J. Voogt, I.J. Schurink, M. Bijvelds, H.R. de Jonge, L.J.W. van der Laan, J. de Jonge, et al., Scaffolds obtained from decellularized human extrahepatic bile ducts support organoids to establish functional biliary tissue in a dish, *Biotechnology and Bioengineering*. 118 836–851 (2021), doi:10.1002/BIT.27613.

[43] A. Papalamprou, C.W. Chang, N. Vapniarsky, A. Clark, N. Walker, L.G. Griffiths, Xenogeneic cardiac extracellular matrix scaffolds with or without seeded mesenchymal stem cells exhibit distinct in vivo immunosuppressive and regenerative properties, *Acta Biomaterialia*. 45 155–168 (2016), doi:10.1016/J.ACTBIO.2016.07.032.

[44] W.C. Jiang, Y.H. Cheng, M.H. Yen, Y. Chang, V.W. Yang, O.K. Lee, Cryo-chemical decellularization of the whole liver for mesenchymal stem cells-based functional hepatic tissue engineering, *Biomaterials*. 35 3607–3617 (2014), doi:10.1016/j.biomaterials.2014.01.024.

[45] E. Ahmed, T. Saleh, M. Xu, Recellularization of Native Tissue Derived Acellular Scaffolds with Mesenchymal Stem Cells, *Cells 2021, Vol. 10, Page 1787*. 10 1787 (2021), doi:10.3390/CELLS10071787.

[46] T. Assis-Ribas, M.F. Forni, S.M.B. Winnischofer, M.C. Sogayar, M. Trombetta-Lima, Extracellular matrix dynamics during mesenchymal stem cells differentiation, *Developmental Biology*. 437 63–74 (2018), doi:10.1016/J.YDBIO.2018.03.002.

[47] Z. Wang, J. Faria, L.C. Penning, R. Masereeuw, B. Spee, Tissue-Engineered Bile Ducts for Disease Modeling and Therapy, *Tissue Engineering - Part C*. 27 (2021), doi:10.1089/ten.tec.2020.0283.

[48] Y. Li, Q. Wu, Y. Wang, L. Li, F. Chen, Y. Shi, J. Bao, H. Bu, Construction of bioengineered hepatic tissue derived from human umbilical cord mesenchymal stem cells via aggregation culture in porcine decellularized liver scaffolds, *Xenotransplantation*. 24 (2017), doi:10.1111/XEN.12285.

[49] Y. Zhang, A. Sharma, D.J. Joo, E. Nelson, A. AbuRmilah, B.P. Amiot, C.J. Boyer, J.S. Alexander, et al., Autologous Adipose Tissue–Derived Mesenchymal Stem Cells Introduced by Biliary Stents or Local Immersion in Porcine Bile Duct Anastomoses, *Liver Transplantation*. 26 100–112 (2020), doi:10.1002/lt.25682.

[50] Y. Zhang, Y. He, S. Bharadwaj, N. Hammam, K. Carnagey, R. Myers, A. Atala, M. Van Dyke, Tissue-specific extracellular matrix coatings for the promotion of cell proliferation and maintenance of cell phenotype, *Biomaterials*. 30 4021–4028 (2009), doi:10.1016/J.BIOMATERIALS.2009.04.005.

[51] P.L. Lewis, J. Su, M. Yan, F. Meng, S.S. Glaser, G.D. Alpini, R.M. Green, B. Sosa-Pineda, et al., Complex bile duct network formation within liver decellularized extracellular matrix hydrogels, *Scientific Reports 2018 8:1*. 8 1–14 (2018), doi:10.1038/s41598-018-30433-6.

[52] G.G. Giobbe, C. Crowley, C. Luni, S. Campinoti, M. Khedr, K. Kretzschmar, M.M. De Santis, E. Zambaiti, et al., Extracellular matrix hydrogel derived from decellularized tissues enables endodermal organoid culture, *Nature Communications 2019 10:1*. 10 1–14 (2019), doi:10.1038/s41467-019-13605-4.

[53] Y.H.K. Yang, C.R. Ogando, C. Wang See, T.Y. Chang, G.A. Barabino, Changes in phenotype and differentiation potential of human mesenchymal stem cells aging in vitro, *Stem Cell Research and Therapy*. 9 1–14 (2018), doi:10.1186/s13287-018-0876-3.

[54] A. Laitinen, M. Lampinen, S. Liedtke, L. Kilpinen, E. Kerkelä, J.-R. Sarkanen, T. Heinonen, G. Kogler, et al., The effects of culture conditions on the functionality of efficiently obtained mesenchymal stromal cells from human cord blood, *Cytotherapy*. 18 423–37 (2015), doi:10.1016/j.jcyt.2015.11.014.

[55] S. Hagmann, B. Moradi, S. Frank, T. Dreher, P.W. Kämmerer, W. Richter, T. Gotterbarm, Different culture media affect growth characteristics, surface marker distribution and chondrogenic differentiation of human bone marrow-derived mesenchymal stromal cells, *BMC Musculoskeletal Disorders*. 30 223 (2013), doi:10.1186/1471-2474-14-223.

[56] S. Jung, A. Sen, L. Rosenberg, L.A. Behie, Human mesenchymal stem cell culture: Rapid and efficient isolation and expansion in a defined serum-free medium, *Journal of Tissue Engineering and Regenerative Medicine*. 6 391–403 (2012), doi:10.1002/term.441.

[57] S.M.G. Fouraschen, S.R.R. Hall, J. De Jonge, L.J.W. Van Der Laan, Support of hepatic regeneration by trophic factors from liver-derived mesenchymal stromal/stem cells, *Methods in Molecular Biology*. 1213 89–104 (2014), doi:10.1007/978-1-4939-1453-1_9.

Appendix A - Protocol isolation of L-MSCs

This protocol is based on the original protocol described in the book 'Animal Models for Stem Cell Therapy', chapter 9: Support of Hepatic Regeneration by Trophic Factors from Liver-Derived Mesenchymal Stromal/Stem Cells [57]

Materials:

- Culture medium
- Ficoll
- PBS

Procedure:

- Collect perfusate in 50 ml tubes and centrifuge 5 min, 1500 rpm, 4 C
- Discard the supernatant and resuspend the cell pellets from all the tubes in 30ml final volume PBS
- Layer the cell suspension on top of 13 ml Ficoll. Drip de cell suspension slowly onto the Ficoll to prevent mixing the two.
- Centrifuge 20 min, 1800 rpm, 20 C, acc. 9, brake 1
- Harvest the enriched cell fraction (ring of cells on the Ficoll) into a new 50 ml tube (with disposable pipette)
- Add PBS to a total volume of 40 ml and centrifuge 5 min, 1500 rpm, 4 C
- Resuspend pellet in medium and count the cells with Trypan Blue (to make a distinction between life and dead cells).
- Seed the cells with a density of 1 - 3.5 cells/cm^2.
- After a few days, some cells will be attached, and a lot of cells will be floating in the medium. Wash away the dead cells and add fresh medium.
- Cells that attach to the plastic and start growing are the MSC. Usually, they have a spindle-like shape and can grow like a normal cell line.

Appendix B - Medium compositions

Advanced DMEM/F12 ++++

Component	Concentration
Advanced DMEM/F12	
HEPES	1M
L-Glutamin	1%
Primocin	500mg/ml
Pen/Strep	10000 U/ml

Start-up medium

Component	Concentration
Advanced DMEM/F12 ++++	
N2	1%
B27	2%
Gastrin I	10 nM
FGF10	100 ng/ml
HGF	25 ng/ml
EGF	50 ng/ml
A8301	5 µM
Nicotinamide	10nM
Forskolin	10 µM
N-Acetylcystein	1,25 mM
R-Spondin	10%
WNT	30%
Noggin	25 ng/ml
Y27632	10 µM
hES cell cloning recovery solution	1:1000 dilution

Expansion medium (EM)

Component	Concentration
Advanced DMEM/F12 ++++	
N2	1%
B27	2%
Gastrin I	10 nM
FGF10	100 ng/ml
HGF	25 ng/ml
EGF	50 ng/ml
A8301	5 µM
Nicotinamide	10nM
Forskolin	10 µM
N-Acetylcystein	1,25 mM
R-Spondin	10%

Differentiation medium (DM)

Component	Concentration
Advanced DMEM/F12 ++++	
N2	1%
B27	2%
Gastrin I	10 nM
FGF10	100 ng/ml
HGF	25 ng/ml
EGF	50 ng/ml
A8301	5 µM
DAPT	10 µM
BMP7	25 ng/ml
Dex	30 µM

MSC medium

Component	Concentration
DMEM/F12	
Non-heat inactivated fetal calf serum (FCS)	10%
Pen/Strep	10000 U/ml

Appendix C - Schematic overview experiments

Schematic overview EM+CM and DM+CM experiments

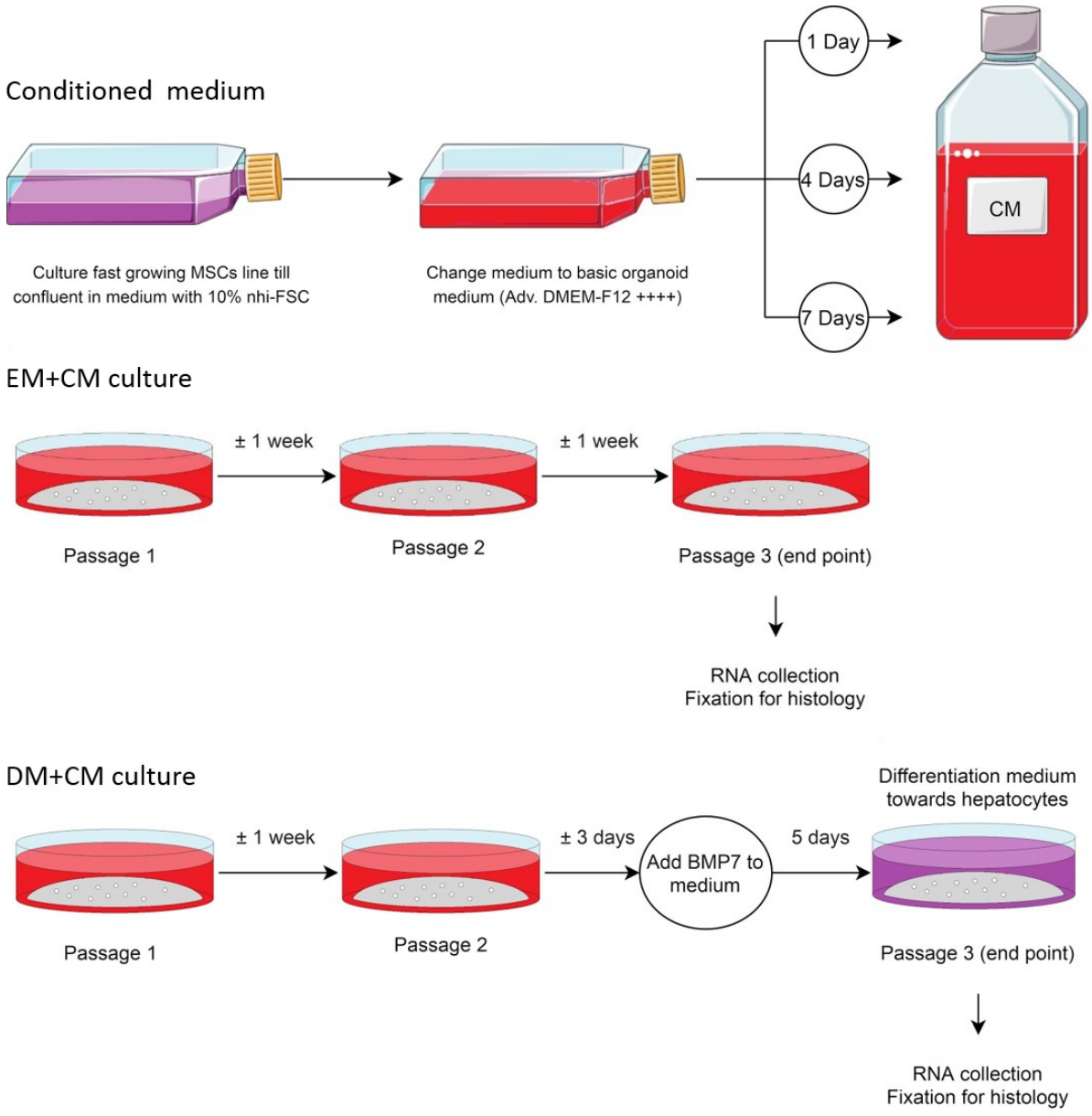

Schematic overview of the direct and indirect co-culture in BME

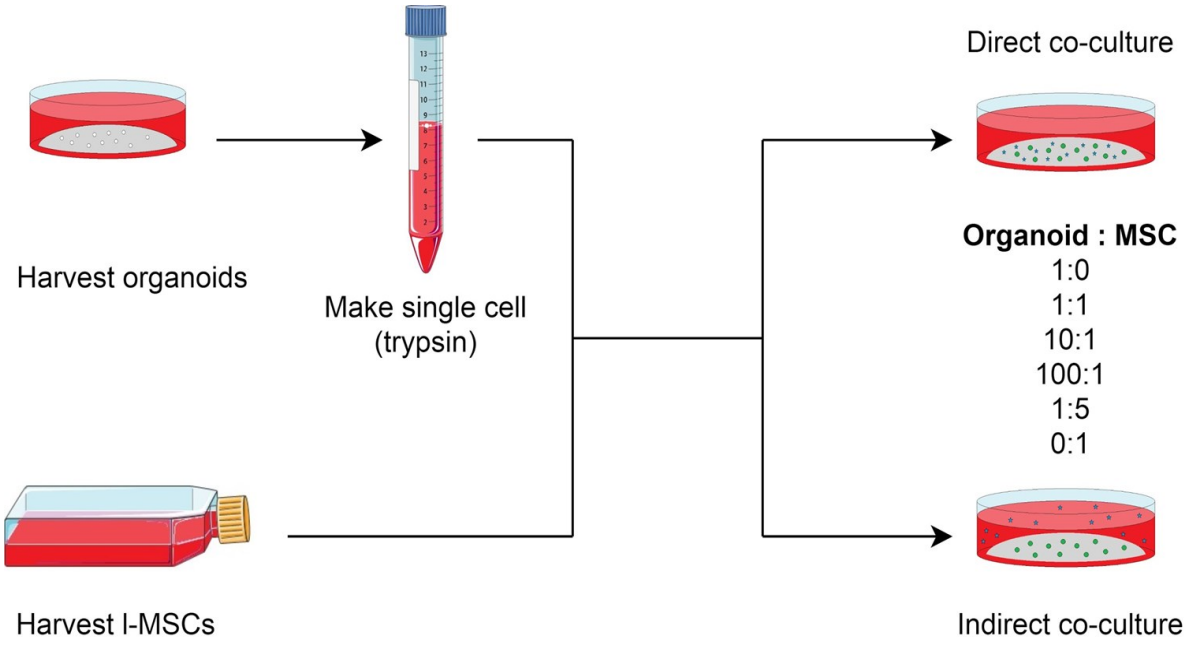

Schematic overview of the direct and MSC-first direct co-culture on liver derived ECM

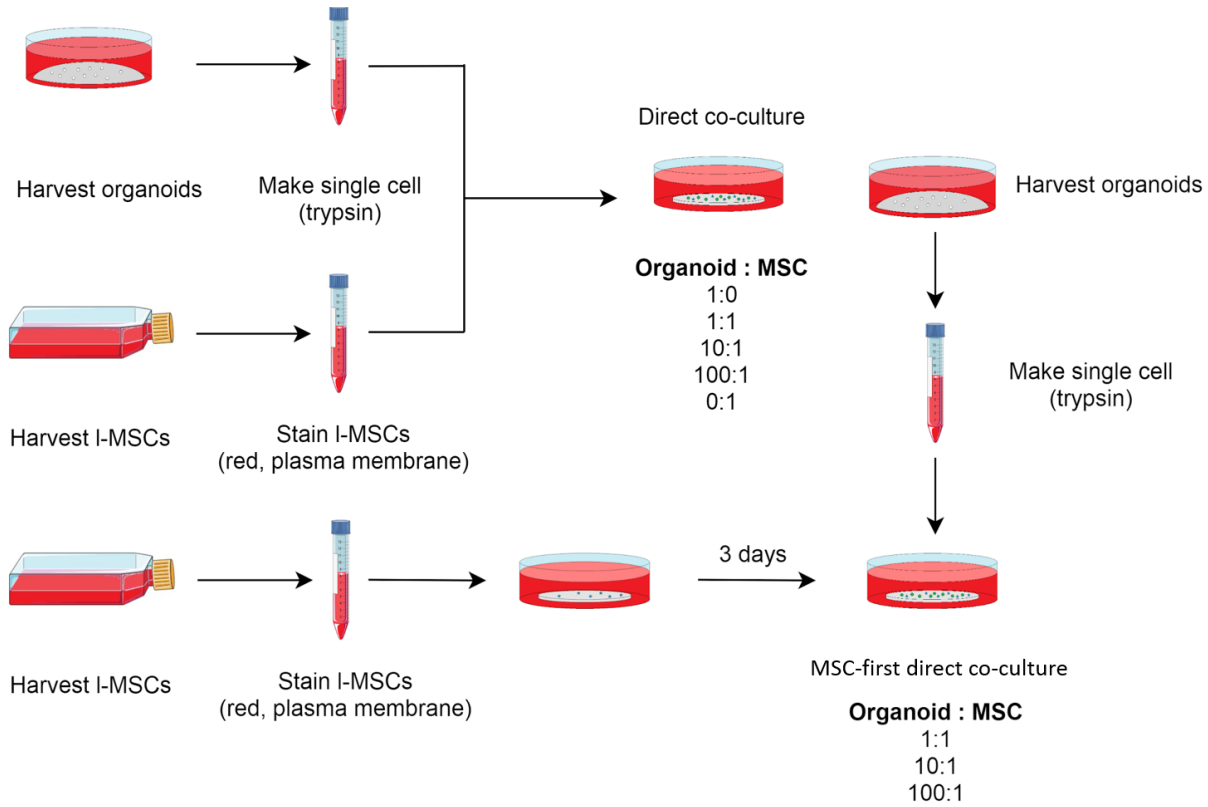

Appendix D - PCR primers

Primer	Forward sequence 5' to 3'	Reverse sequence 5' to 3'
GAPDH	CTTTTGCGTCGCCAGCCGAG	CCAGGCGCCCAATACGACCA
HPRT-1	ACCAGTCAACAGGGGACATAA	CTTCGTGGGGTCCTTTTCACC
B2M	GTGTCTGGGTTTCATCCATC	GGCAGGCATACTCATCTTTT
LGR5	GTCAGCTGCTCCCGAATCCC	TGAAACAGCTTGGGGGCACA
CK7	GGGGACGACCTCCGGAATAC	CTTGGCACGCTGGTTCTTGA
CK19	GCACTACAGCCACTACTACACGA	CTCATGCGCAGAGCCTGTT
EPCAM	GACTTTTGCCGCAGCTCAGGA	AGCAGTTTACGGCCAGCTTGT
KI67	CTACGGATTATACCTGGCCTTCC	AGGAAGCTGGATACGGATGTCA
Vimentin	CGGGAGAAATTGCAGGAGG	TGCTGTTCCTGAATCTGAGC
Albumin	CTGCCTGCCTGTTGCCAAAGC	GGCAAGGTCCGCCCTGTCATC
CYP3A4	AGCAAAGAGCAACACAGAGCTGAA	CAGAGGTGTGGGCCCTGGAAT
CD105	CCACTAGCCAGGTCTCGAAG	GATGCAGGAAGACACTGCTG
CD90	ATGAACCTGGCCATCAGCA	GTGTGCTCAGGCACCCC

Appendix E - Brightfield images of CM co-cultures

Brightfield images of EM+CM ICOs

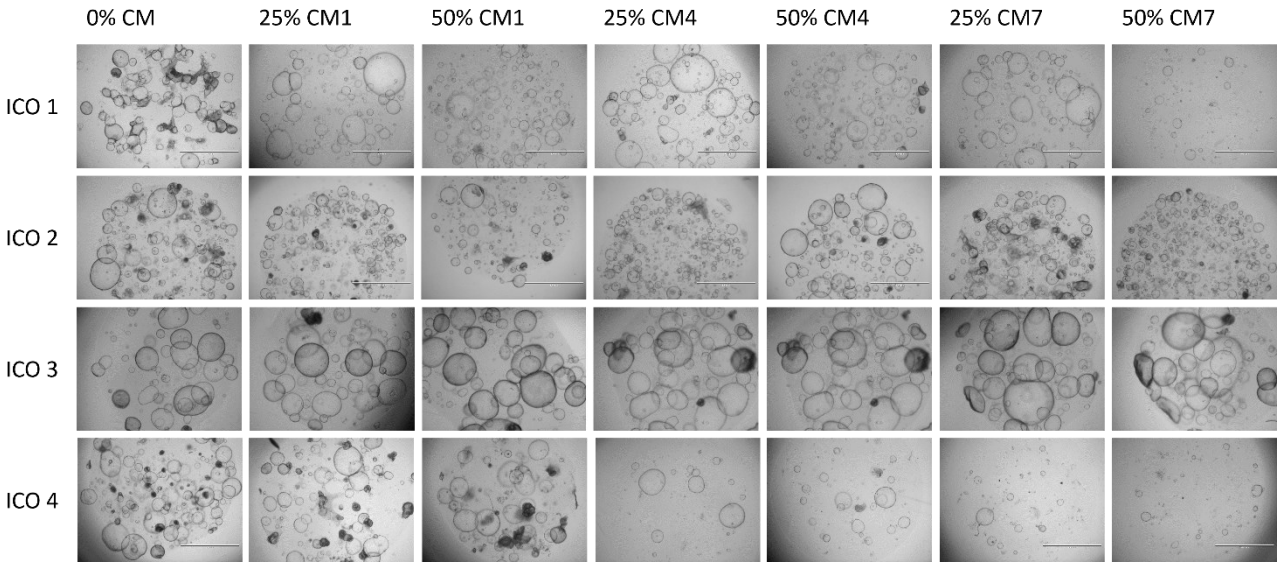

Brightfield images of EM+CM versus DM+EM ICOs

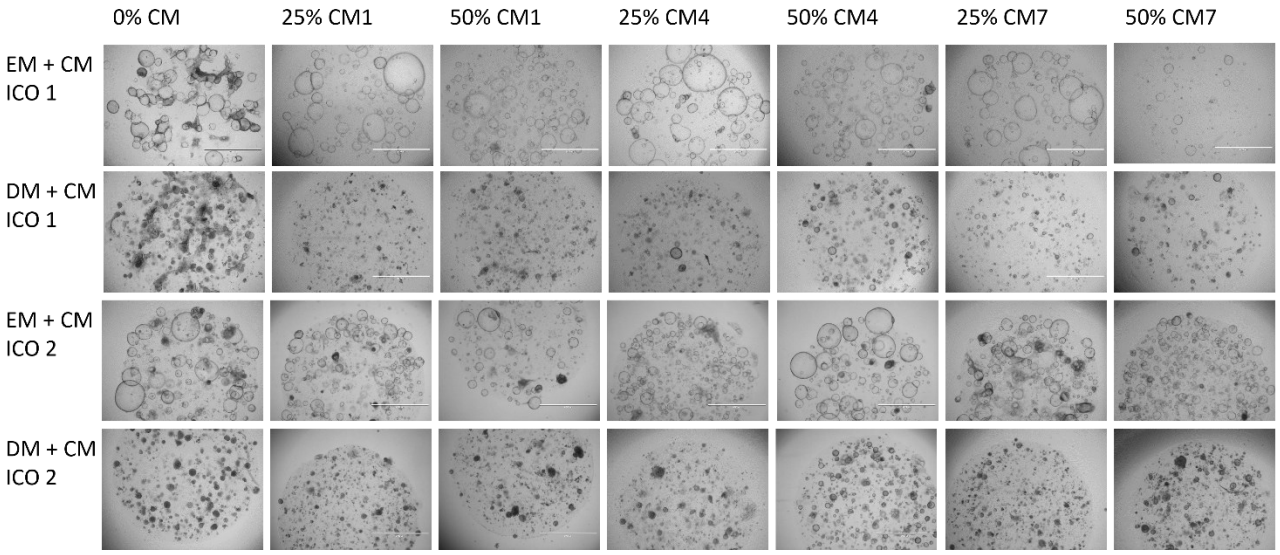

Appendix F - Brightfield images of BME co-cultures

Brightfield images of day 21 of the direct co-culture in BME

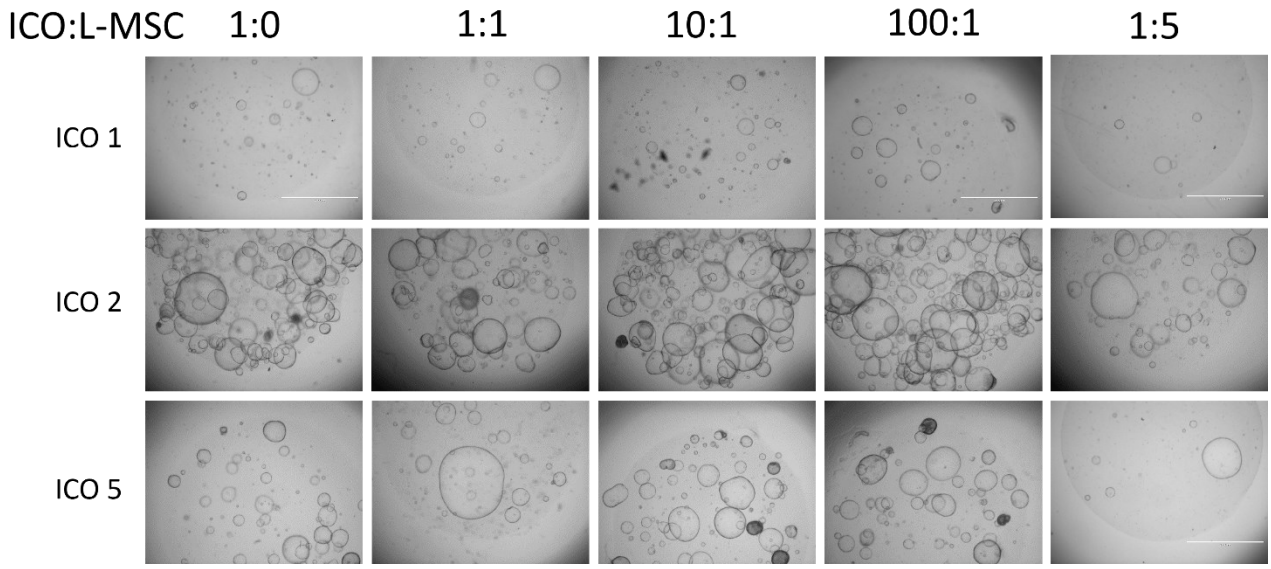

Brightfield images of day 21 of the indirect co-culture in BME

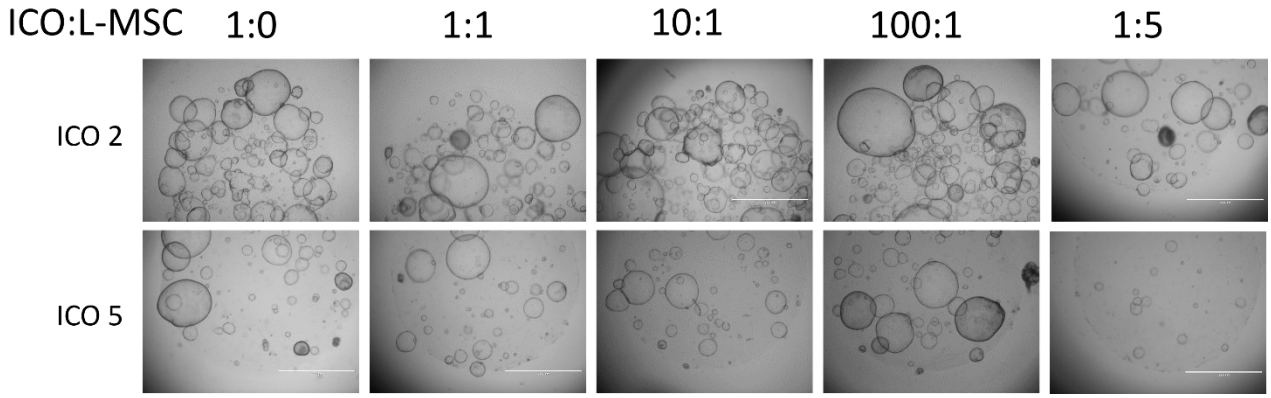

Appendix G - Brightfield images of ECM co-cultures

Brightfield images of day 21 of the direct and MSC-first direct co-culture on ECM

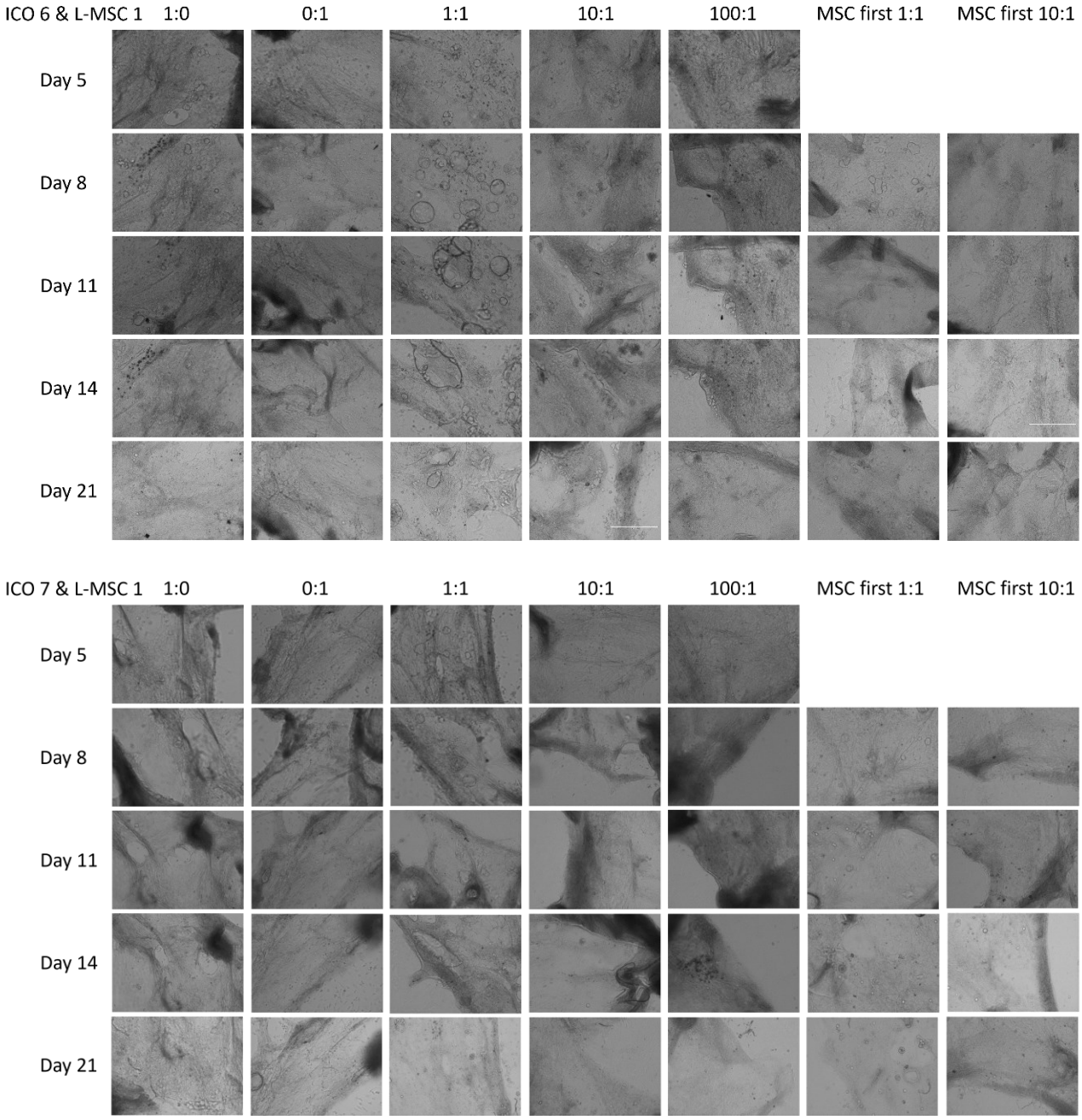

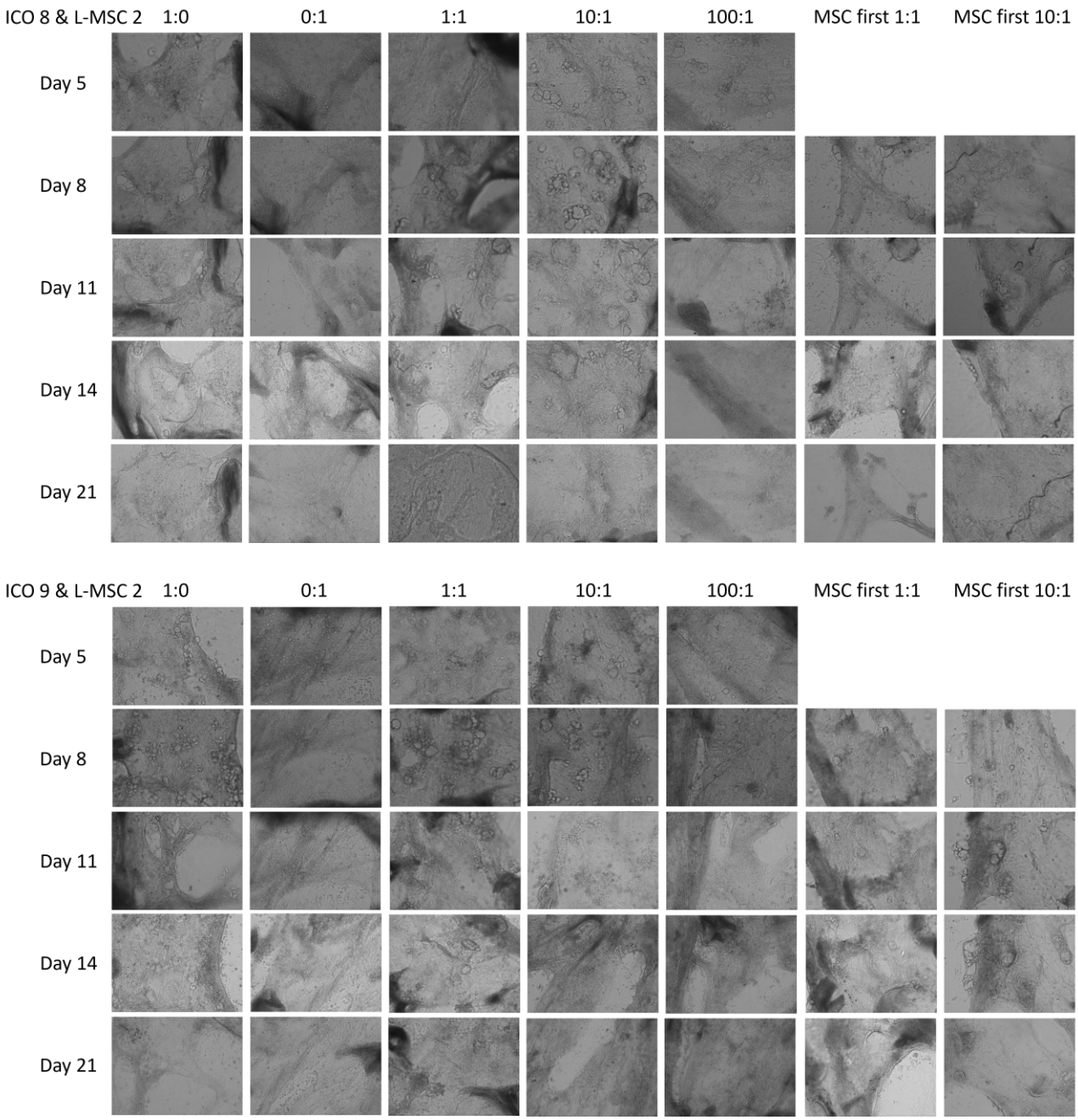
ICO 8 & L-MSC 2
1:0
0:1
1:1
10:1
100:1
MSC first 1:1
MSC first 10:1
Day 5
Day 8
Day 11
Day 14
Day 21
ICO 9 & L-MSC 2
1:0
0:1
1:1
10:1
100:1
MSC first 1:1
MSC first 10:1
Day 5
Day 8
Day 11
Day 14
Day 21

Appendix H - Brightfield images of blast forming

Brightfield images of blast forming in the direct co-cultures on ECM